# Optimizing Protocols for Combining Imaging Mass Spectrometry (IMS) and Optical Imaging of Traditionally Histologically Stained Tissues: Advancements in Single-Cell Analysis Using IMS

Ameh Great Orotomah

A Thesis

in

The Department

of

Chemistry and Biochemistry

Presented in Partial Fulfillment of the Requirements for the Degree of Master of Science (Chemistry/Biochemistry) at Concordia University,

Montreal, Quebec, Canada

# **CONCORDIA UNIVERSITY**

# **School of Graduate Studies**

This is to certify that the thesis prepa	red
--	-----

By:	Ameh Grea	at Orotomah	
Entitled:	Optimizing Protocols for Combining Imaging Mass Spectrometry (IMS) and Optical Imaging of Traditionally Histologically Stained Tissues: Advancements in Single-Cell Analysis Using IMS		
and submit	ted in partial fulfillment of the requ	irements for the degree of	
	Master of Science (Ch	nemistry Biochemistry)	
complies wand quality		neets the accepted standards regarding originality	
Signed by	the final Examining Committee:		
		Chair	
-	Melissa K. Passarelli	-	
-		_ Examiner	
	Cameron Skinner		
-	Alisa Piekny	- Examiner	
-	Melissa K. Passarelli	- Supervisor	
Approved	by		
	Chair of Department or	Graduate Program Director	
	2025		
	Dean of Faculty		

#### **Abstract**

Optimizing Protocols for Combining Imaging Mass Spectrometry (IMS) and Optical Imaging of Traditionally Histologically Stained Tissues: Advancements in Single-Cell Analysis Using IMS.

#### Ameh Orotomah

Biomolecular changes linked to disease can be studied by integrating Imaging Mass Spectrometry (IMS) with histopathology. However, co-registering IMS with optical images of stained tissues is challenging due to sample preparation constraints and resolution discrepancies, particularly as IMS advances toward single-cell resolution. This work evaluates workflows for multimodal tissue analysis (sequential vs. consecutive) by combining IMS with histological imaging and incorporating laser-etched indium tin oxide (ITO) slides to improve image registration at the cellular level.

In this study, coronal mouse brain tissues were analyzed using cluster ion beam secondary ion mass spectrometry (SIMS) and/or matrix-assisted laser desorption/ionization (MALDI) mass spectrometry. For high-resolution MALDI imaging, 1,5-diaminonaphthalene matrix was sublimated on the tissue sections. Traditionally, serial tissue sections have been used for

hematoxylin and eosin (H&E) staining and IMS image co-registration. Here, we examine the benefits and caveats of staining the same tissue section post-IMS analysis.

The 35 µm spatial resolution of our TOF-MALDI instrument exceeds the average diameter of a mouse brain cell, limiting single-cell multimodal IMS analysis. To overcome segmentation challenges, we employed Cell Segmentation Globally Optimized (CSGO), an open-source deep learning model specifically optimized for histological images, which enables accurate and automated whole-cell segmentation from optical microscopy of H&E-stained tissue images. While consecutive sections align overall tissue structure, they fail at cellular precision due to misalignment. By combining deep learning-based segmentation with same-section multimodal coregistration using laser-etched fiducial markers, we achieved improved spatial alignment for high-resolution molecular mapping, advancing disease characterization and biomarker discovery.

#### Acknowledgment

First, I thank God Almighty for the strength, wisdom, and perseverance to complete this work. Without His grace, this journey would not have been possible.

I am deeply grateful to my supervisor, Dr. Melissa Passarelli, for her invaluable guidance and support during my research. Your mentorship has been key to my growth, both academically and professionally.

I also want to thank my committee members, Dr. Alisa Piekny and Dr. Cameron Skinner. Your thoughtful feedback and expertise greatly enhanced the quality of this thesis.

To my friends, Adriana Reitano, Joshua Osagu, Milad Ezzati, Samaneh Naghibalhossaini, and my entire lab group, thank you for your encouragement, support, and insightful discussions. Sharing the ups and downs of this journey made it much more meaningful.

Lastly, I appreciate the faculty and staff of the Department of Chemistry and Biochemistry. Each of you has positively impacted my life, and I appreciate the sense of community and professionalism that I have experienced throughout my time here.

# **Table of Contents**

List of Figures	Viii
List of Equations	X
List of Abbreviations	xi
Chapter 1 : Introduction	1
1.1 Imaging Mass Spectroscopy (IMS)	1
1.1.1 Secondary Ion Mass Spectrometry (SIMS)	2
1.1.2 Matrix-assisted laser desorption ionization (MALDI)	3
1.1.3 Desorption electrospray ionization (DESI)	4
1.1.4 Multi-modal IMS challenges and advantages over traditional clin	ical chemical imaging
1.2 Overview of Traditional Histology	
1.2.1 Tissue Sectioning	
1.2.2 Tissue Staining	10
1.3 Mounting medium (Aqueous and Organic)	11
1.4 Integrating IMS with Histologically Stained Tissue	12
1.5 Challenges of Coregistering	14
1.6 Thesis Aims and Objectives	16
Chapter 2 : Research Methodology	17
2.1 Methodology of Integration	17
2.1.1 Same tissue vs adjacent tissue workflow	18
2.1.2 Laser-etched fiducial markers for co-registrations	20
2.2 Secondary ion mass spectrometry (SIMS) Analysis	20
2.2.1 Instrumentation and parameters	21
2.3 Matrix-assisted laser desorption ionization (MALDI) Analysis	21
2.3.1 Matrix deposition	22
2.3.2 Instrumentation and parameters	22
2.4 Hematoxylin and Eosin Staining	23
2.4.1 Light Microscopy	

Chapter 3: Results	26
3.1 Data Formats	26
3.2 Image Processing using R programming language	27
3.3 Image Processing using MATLAB	30
3.4 Image Registration	32
3.4.1 Jaccard Similarity	36
3.5 Single-cell Segmentation	38
Chapter 4 : Discussion and Future Direction	46
4.1 Summary	46
4.2 The Role of Integrated Tissue Analysis in Molecular Pathology	48
4.3 Possible Future Direction	50
References	52

# **List of Figures**

Figure 1 Prototype microscope slide etched using a Rayjet desktop laser engraver (Trotec)
equipped with a 30W CO <sub>2</sub> laser, which features a spatial resolution of 400 μm
Figure 2 Schematic representation of our workflow.
Figure 3.a) Modified H&E staining protocol and b) H&E-stained optical image of the
hippocampus region of mouse brain tissue (scale bar =50 $\mu$ m).
Figure 4.a) Mean spectra of Multimodal IMS mouse brain tissue section 1 and b) zoomed in
spectra highlighting lipid peak dipalmitoyl phosphatidylcholine (DPPC) with the blue arrow 28
Figure 5. a) MALDI-ToF mean spectrum of mouse brain tissue section 3, b) zoomed view
highlighting dipalmitoyl phosphatidylcholine (DPPC), and c) zoomed view highlighting
galactosylceramide (GalCer), both indicated by blue arrows
Figure 6.a) MALDI-ToF ion image of DPPC (m/z 734) in multimodal IMS mouse brain tissue
section 1, b) DPPC ion image in mouse brain tissue section 3, and c) GalCer (m/z 826) ion image
in mouse brain tissue section 3
Figure 7.a) ToF-SIMS mean spectra from multimodal IMS mouse brain tissue section 1, with
annotated fragments: m/z 86 and 184 (phosphocholine head group) and m/z 369 (cholesterol); b)
corresponding ion images for m/z 86, 184, and 369 (left to right), illustrating their spatial
distribution within the tissue
Figure 8.a) H&E-stained mouse brain tissue section 2, b) H&E-stained multimodal IMS mouse
brain tissue section 1, and c) registered H&E-stained mouse brain tissue section 2 overlayed onto
H&E-stained multimodal IMS mouse brain tissue section 1

Figure 9. Same-tissue coregistration of ion images for phosphocholine fragments (m/z 86 and
184), cholesterol (m/z 369), and DPPC (m/z 734) onto the coordinates of the H&E-stained
multimodal IMS mouse brain tissue section 1
Figure 10. a) H&E-stained multimodal IMS mouse brain tissue section 1, b) H&E-stained
mouse brain tissue section 2, <b>c-d</b> ) color deconvolution of sections 1 and 2, respectively, <b>e-f</b> )
threshold-segmented hematoxylin channels from sections 1 and 2, respectively, and g) overlay of
the segmented masks from both sections
Figure 11.a) H&E-stained multimodal IMS mouse brain tissue section 1, b) cropped region from
(a) highlighting the area of interest
Figure 12.a) Cropped H&E-stained multimodal IMS mouse brain tissue section 1, b) nuclei
segmentation, c) membrane segmentation of the cropped region, and d) final watershed-
segmented result
Figure 13.a) Watershed-segmented H&E-stained multimodal IMS mouse brain tissue section 1,
b) cropped region of the same section, and c) isolated whole cells extracted from the cropped
area
Figure 14. a-c) Overlay of isolated cell boundaries on the cropped, registered ToF-SIMS mouse
brain ion images for m/z 86, 184, and 369, respectively; <b>d-f)</b> corresponding mass spectra for each
cell 43

# **List of Equations**

Equation 1. Fixed point equation	32
Equation 2. Homography equation	33
Equation 3. Homography equation (standard form)	33
Equation 4. Jaccard Index	36

#### **List of Abbreviations**

CSGO Cell Segmentation Globally Optimized

DESI Desorption Electrospray Ionization

DPPC Dipalmitoyl phosphatidylcholine

H&E Hematoxylin and Eosin

IMS Imaging Mass Spectrometry

LMIG Liquid Metal Ion Gun

MALDI Matrix-Assisted Laser Desorption

MALDI-ToF Matrix-Assisted Laser Desorption-Time of Flight

MATLAB Matrix Laboratory

ORO Oil Red O

PC Phosphocholine

SIMS Secondary Ion Mass Spectrometry

ToF-SIMS Time of Flight-Secondary Ion Mass Spectrometry

#### **Chapter 1: Introduction**

#### 1.1 Imaging Mass Spectroscopy (IMS)

Imaging mass spectrometry (IMS) is a series of techniques capable of providing spatially resolved molecular mass spectrometric analyses, which allows for the visualization of molecules on complex surfaces.[1] The primary advantage of IMS over other imaging techniques, such as immunochemistry and fluorescence microscopy, is its untargeted approach, which requires no labeling of any particular compound or class of compounds.[2] However, combining IMS technologies with these other analytical approaches provides a more effective means to probe the molecular complexity of biological systems.[3] A variety of technologies have emerged within the field of IMS, utilizing different ionization methods to generate ion maps of a specific sample.[4] Three of the most prominent imaging mass spectrometry techniques are Secondary Ion Mass Spectrometry (SIMS), Matrix-Assisted Laser Desorption Ionization (MALDI), and Desorption Electrospray Ionization (DESI).[5]

The emergence of MALDI-based IMS has found extensive applications in biological research and drug development, introduced in the early 2000s by Caprioli *et al.* [6] and Spengler and Coworkers.[6] Since its introduction, IMS has been widely applied to visualize various biomolecules. For example, it has been used to visualize biomolecules, such as peptide deposition for Alzheimer's disease in both mice and the human brain tissue [8], and to identify the lipid signature of advanced human carotid atherosclerosis.[7] IMS has also been employed to identify 74 and 147 unique lipids in sclerosis lesions of mouse kidneys and human brains, respectively.[8] Additionally, it has been used to investigate changes in neutral lipid composition between healthy and diseased human skin tissue.[9] Beyond its role in biological research, IMS has significant applications in pharmaceuticals, particularly in studies of drug absorption and distribution. For

instance, it has been used to study the oral absorption of three FDA-approved drugs (atenolol, metoprolol, and propranolol) in the gastrointestinal tract of rats.[10] Moreover, IMS has enabled the generation of quantitative skin distribution profiles by determining the tissue extinction coefficients (TEC) of topically administered molecules-roflumilast, tofacitinib, ruxolitinib, and LEO 29102-across human skin cross-sections.[11]

#### 1.1.1 Secondary Ion Mass Spectrometry (SIMS)

SIMS is a surface analysis technique in which an energetic beam of ions, traditionally Ar+, Ga+, or alkali metal ions, is directed at the surface of a sample. In the process, the primary ions transfer their energy to molecules on the surface, dislodging secondary ions.[12] These sputtered particles are ejected as neutral atoms and molecules, as well as electrons and ions.[13] There are two main modes of analysis in SIMS: static (represented by ToF-SIMS) and dynamic (represented by NanoSIMS).[14] Although both methods involve analyzing secondary ions emitted from the sample's surfaces, they differ in the configurations of their ion optics, primary ion sources, and mass analyzers.[15] Static SIMS is such that the total primary ion dose does not exceed the static limit, 10<sup>13</sup>ions/cm<sup>2</sup>, to maintain molecular sensitivity to the uppermost monolayers, minimize sample damage, and promote the desorption of large organic fragments.[13] In dynamic SIMS, relatively large amounts of material are removed because the primary ion dose exceeds the so-called "static limit."[16]

Two broad classes of instruments exist for constructing secondary ion images: ion microscopes and ion microprobes. In the microprobe approach, a primary ion beam is used to raster scan a predefined area, and the acquired mass spectrum is stored along with the spatial coordinates of each spot.[17] The molecular images are then reconstructed from the individual mass spectra after

the experiment is completed.[18] For ion microscopes, surface molecules are desorbed simultaneously in a relatively large area, typically 200-300 µm in diameter. These ion images in imaging mass spectrometry (IMS) represent the spatial intensity distribution of a specific *m/z* signal, which can be assigned to a particular compound.[19] Essentially, an ion image displays a heat map rendered using a color map of choice.[20] SIMS offers excellent sensitivity in the parts per million to parts per billion range, combining the ability to produce mass spectra from sample surfaces with images having lateral resolution down to 50 nm.[21][22] The high sensitivity and spatial resolution of ToF-SIMS make it a valuable tool for studying biological samples, and the method has been applied to a wide range of samples in the life sciences.[23] For example, ToF-SIMS has been used to image lipids in rat brains [24], investigate the distribution of hippocampal zinc in rat brains [25], and quantify cholesterol in the cerebral cortex of Alzheimer's disease patients.[26]

#### 1.1.2 Matrix-assisted laser desorption ionization (MALDI)

Matrix-assisted laser desorption/ionization (MALDI) is one of the two "soft" ionization techniques, alongside electrospray ionization (ESI), which enables the sensitive detection of large, non-volatile, and labile molecules by mass spectrometry.[27] MALDI mass spectrometry imaging enables label-free, in situ analysis of chemical compounds directly from the surface of two-dimensional biological tissue slices.[28] In this technique, a high energy UV laser is used to ablate the sample surface that has already been added to a matrix, and the analyte is assumed to be homogeneously embedded in a matrix material, which absorbs the laser energy and is responsible for the transfer of the analyte into the gas phase without thermal stress.[29] Matrix deposition is a crucial aspect in determining the success of MALDI-IMS experiments, as uniform matrix

application is essential to minimize variations in analyte extraction and desorption.[30] Although a large number of MALDI matrices have been identified over the years, most analysts seem to rely on a relatively small set, typically one to two dozen established compounds.[31] The actual choice of matrix to use for the analysis depends on the type of sample being analyzed, with common ones being derivatives of benzoic or cinnamic acid, such as 2,5-dihydroxybenzoic acid (2,5-DHB).[32] In the last decade, matrix-assisted laser desorption/ionization time-of-flight mass spectrometry (MALDI-ToF MS) has been widely used as an analytical chemistry tool for the detection of large and small molecules (e.g., polymers, proteins, peptides, nucleic acids, amino acids, lipids, etc.) and clinical analysis and research (e.g., pathogen identification, genetic disorders screening, cancer diagnosis, biomarker discovery, etc.[33] For instance, MALDI-ToF has been applied to discover potential biomarkers for childhood absence epilepsy using BS/Orl (seizure-prone) and BR/Orl (seizure-resistant) inbred mouse strains, which differ in their susceptibility to epileptic seizures[34], [35], and image peptides in mouse brain tissue with mass accuracies of up to 6 ppm and a spatial resolution of 200 µm. [36] MALDI mass spectrometers routinely enable the analysis of femtomole amounts of basic (e.g., tryptic) peptides with mass accuracies in the low-ppm range and lateral resolution of 20-200 µm.[37]

#### 1.1.3 Desorption electrospray ionization (DESI)

In DESI, electrically charged droplets are directed at the sample of interest, where ions are generated from the sample constituents and directed into a commercial mass spectrometer, [38] Because it can operate in ambient conditions (room temperature and atmospheric pressure) and its limited sample preparation requirements. [39] The imaging experiments are performed by moving the tissue surface in the x and y directions under the impinging spray of charged microdroplets

with step motors. The pixel-to-pixel mass spectra can be plotted as a two-dimensional image, allowing biochemical mapping of the tissue.[40] The typical spatial resolution of DESI IMS, approximately 1 mm using manual sample control[41], has been improved by increasing the outer diameter of the spray capillary and utilizing a positioning disk within the DESI source, resulting in a spatial resolution of 20 µm. [42] Samples can be directly spotted or deposited on a solid surface for analysis. In the case of tissue sections, imaging analysis is typically performed on a single piece of tissue, typically 5-25  $\mu$ m thick, which is mounted onto a glass slide and stored at -80°C until analysis. [43] The DESI method has high sensitivity and is virtually instantaneous in response time, making it applicable to the analysis of proteins and protein complexes, carbohydrates and oligonucleotides, as well as industrial polymers and small organic molecules.[44] Lipidomics, metabolomics, and drug development are key areas in ambient mass spectrometry imaging for profiling and spatially mapping endogenous and exogenous molecules in biological tissues.[45] Using DESI, temporal changes in lipid profiles occurring within mouse ovaries during the ovulatory cycle have been characterized. [46] Campbell et.al, using DESI, revealed that the level of sulfatide in the middle molecular layer was significantly higher than that in the granule cell layers and the inner molecular layer of the rat hippocampus dentate gyrus.[47] Using this technique, a stratified random survey was conducted to assess the proportion of poor-quality oral artesunate, an antimalarial drug for Plasmodium falciparum malaria, sold at medicine outlets in the Lao People's Democratic Republic, highlighting its impact on treatment failure and drug resistance.[48]

# 1.1.4 Multi-modal IMS challenges and advantages over traditional clinical chemical imaging

Imaging mass spectrometry has proven to be a valuable tool over the years for mapping molecules, such as peptides, lipids, and drugs, in biological samples. Although very useful on its own, this technique can be combined with other imaging modalities to obtain complementary information, thereby enhancing the characterization of biological samples. Scientists can leverage the molecular detectability of mass spectrometry and the spatial resolution of imaging techniques, such as histopathology and immunohistochemistry, to obtain information on the qualitative, quantitative, and spatial distribution of molecules without the need for labeling.[49] However, multimodal approaches possess challenges such as non-standardized characteristics, custom software, inadequate commercial support, and integration issues with other instruments that need to be addressed. One of the primary challenges associated with multimodal IMS techniques is image registration, which involves overlaying images (two or more) of the same location taken at different times, from different viewpoints, and/or by different detectors.[50] Imaging modalities such as DESI, MALDI, and SIMS produce images with different spatial resolutions, sensitivities, and dynamic ranges. Reasonable image registration and data integration require advanced data processing, which includes considering tissue deformation and signal enhancement, extracting qualitative, quantitative, and spatial location information, identifying complementary information, and optimizing fusion strategies. [49] The interpretation of vast amounts of data produced by multimodal IMS approaches also presents unique challenges. Data analysis tools, such as principal component analysis (PCA) and non-negative matrix factorization (NMF)[51], which facilitate the interpretation and comparison of images, should be employed.[51]

Despite these challenges, multi-modal IMS offers several advantages over traditional clinical chemical imaging techniques. One significant advantage is its ability to deliver comprehensive and detailed spatial information on molecules of interest across different length scales, ranging from the cellular to the multi-cellular level and from organs to whole biological systems.[52] Furthermore, label-free multimodal imaging will impact analytical chemistry, especially the "omics" sciences, for two main reasons: (1) the imaging techniques provide complementary information that identifies molecules and validates results, and (2) the spatial and spectral information has boosted the value. In addition to individual imaging techniques, the combination and integration of several imaging techniques, known as multimodal imaging, can provide extensive anatomical, functional, and molecular information, thereby accelerating drug discovery and development processes.[53] Additionally, this enables comprehensive molecular mapping of tissues, aiding in the discovery of biomarkers for diseases such as cancer and neurodegenerative disorders.[54]

#### 1.2 Overview of Traditional Histology

Traditional histology is the scientific study of tissue structure and organization, using microscopic examination with light, fluorescence, or electron microscopes.[55] It examines a thin slice or section of tissue that has been previously prepared using appropriate histological techniques.[56] While histology provides key information about biological tissue, animal growth, physiology, and disease tissue, histopathology examines the normal cellular structure of tissue and looks for abnormalities.[57] Typical steps include tissue preparation such as extraction, embedding & fixing, sectioning, staining, and evaluation under a microscope to identify normal and diseased states. [58] This technique has been crucial in pathology for over a century, playing a vital role in

disease diagnosis, understanding tissue structure, and evaluating treatment efficacy. The process typically begins with a sample collection, which can take the form of a biopsy, surgical excision, or autopsy. To preserve the sample as close to its natural state as possible in preparation for further processing and examination, samples are fixed using chemicals such as formaldehyde or glutaraldehyde. [59] Fixatives enhance the preservation of tissues and cells through an irreversible process of cross-linking proteins. After fixation, the sample is passed through a series of ethanol to dehydrate the tissue and harden it further for microscopic evaluation, followed by clearing with xylene. Xylene is miscible with ethanol, ensuring its removal from the sample. [60] Following clearing, the sample is embedded in paraffin wax, creating a block of tissue that facilitates easy sectioning using a microtome. The paraffin-embedded tissue block is sectioned into thin slices, mounted onto a glass slide, and then stained before being evaluated using a microscope. However, "frozen section" is an alternative tissue preparation technique where, in contrast to routine processing, is a rapid histological examination done on fresh tissue[61], as the process of fixation and embedding of biological material in paraffin and other media may destroy certain components, particularly enzymes, fats, and some antigen sites.[62] Staining of tissues is a vital step in histology, used to highlight important features of the tissue and enhance tissue contrast, as most tissues appear colorless.[63] The hematoxylin and eosin (H&E) stain is the standard used for microscopic examination of tissues that have been fixed, processed, embedded, and sectioned.[64]The H&E procedure stains the nucleus and cytoplasm with contrasting colors, allowing for the easy differentiation of cellular components. [65] Examples of some common kinds of stains include oil red o (ORO), periodic acid-Schiff, Giemsa, and Masson's trichrome. [66] While the field of traditional histology has been useful in medical diagnosis, scientific study, autopsy, and forensic investigation, it can only provide structural and morphological information.

It cannot provide molecular information about the sample being analyzed. However, recent developments, such as digital pathology and integration with molecular imaging techniques, continue to enhance the capabilities and applications of traditional histology.

#### 1.2.1 Tissue Sectioning

Microscopic analysis of cells and tissues requires the preparation of very thin, high-quality sections (slices) mounted on glass slides and appropriately stained to demonstrate normal and abnormal structures.[67] Sectioning is the process of cutting tissue into thin slices. Tissue is typically embedded with optimal cutting temperature (OCT) or paraffin before being sectioned for analysis.[68] There are two main categories of sectioning: paraffin or frozen sectioning. Paraffin sectioning is a procedure that involves cutting thin slices of dehydrated and infiltrated tissue with wax using specialized equipment.[69] Paraffin sectioning is the most common histological technique applied in preparing tissue sections. It not only observes the form and structure of normal cells, but it is also the major pathological and forensic scientific method applied for studying, observing, and determining changes in the form of cellular tissues.[70] Paraffin sections require extensive fixation and processing steps, but they provide superior morphology compared to other sectioning methods.[71] On the other hand, the frozen section is a rapid tissue section of a tissue that has been frozen directly to harden it, providing an immediate report on the tissue sample. [72] Frozen sections are performed using an instrument called a cryostat, a refrigerated device that contains a microtome. [73]In this procedure, fresh tissue is commonly plunged into a suitable cryoagent (such as liquid nitrogen-cooled isopentane) immediately after being excised from the gross specimen, placed on a cryostat chuck, and then frozen. It is then embedded at -20 °C in a suitable medium, such as an optimal cutting temperature (OCT) compound.[74] The method has several

advantages, namely: (a) it takes up much less time than the regular paraffin method; (b) since the tissue is not dehydrated, the cells retain a life-like appearance with little shrinking; and (c) the tissues can be sectioned, if necessary, without any fixation at all.[75] The Practical Guide to Specimen Handling in Surgical Pathology recommends a section thickness of 4-5 μm for paraffin sections and, [76] 4-7 μm optimal cutting thickness for frozen sections.[77]

Tissue sectioning is a fundamental procedure in traditional histology. This process provides thin slices of either paraffin-embedded or frozen tissue for staining and microscopic analysis. Reproducible, high-quality cutting of tissues preserves the tissue's morphology, enabling researchers and pathologists to accurately assess the tissue's condition, detect abnormalities, and draw conclusions from their observations.

#### 1.2.2 Tissue Staining

Staining is the process of coloring tissues by using dye.[78] Histological staining chemically introduces contrast into tissue sections, which can then be analyzed and used to screen for diseases through bright-field microscopic imaging of the stained samples.[79] They are classified into 2 categories: routine and special stains.[80] Routine staining primarily refers to the hematoxylin and eosin (H&E) stain, while special staining refers to alternative techniques used to provide specific information that researchers or pathologists need beyond the routine H&E stain.[81] The H&E is the most commonly used stain for pathology diagnosis.[68] As the name implies, it is the combination of two separate dyes, namely, hematoxylin and eosin. H&E staining involves staining with hematoxylin, a basic dye that stains acidic structures with a purple/blue hue, such as nuclear components, and eosin, an acidic dye that stains basic structures, resulting in a pink/red hue for the cytoplasm.[82] A typical H&E staining procedure includes hydrating and fixing the tissue

using alcohol, further hydration of the tissue using water, staining with hematoxylin, differentiation step using acid alcohol to remove excess background hematoxylin stain, rinsing in water to stop the acid alcohol reaction, bluing step to change the reddish-purple hematoxylin into a darker bluish-purple using a weak alkaline solution, for example, Scott's tap water, subsequently rinsing with water to remove bluing agent in preparation for eosin staining, counterstaining with eosin to differentiate cellular components, differentiate and dehydrating the tissue section in increasing concentration of alcohol, before applying a mounting medium and coverslipped using a thin glass slide.[83] Special stains may be requested to confirm or aid in diagnosis and to define specific cells, structures, and compounds.[84] Some examples of special stains, according to their application in specific tissues, include periodic acid-Schiff (PAS) for visualizing carbohydrates in tissue, Sudan and Oil Red O (ORO) dye for staining lipids, cresyl violet stain for the nervous system, and acid-fast bacteria stain for microorganisms.[85]

H&E-based tissue staining is particularly useful in identifying morphological changes associated with cancer and other disease states.[86] However, the choice of staining method depends on the research or clinical diagnostic needs, with some stains targeting general tissue architecture and others designed for specific molecular markers, as mentioned earlier.

#### 1.3 Mounting medium (Aqueous and Organic)

The mounting medium is the solution in which the specimen is embedded, typically under a glass coverslip. [87] This can be a liquid, gum, or resinous material that is soluble in water, alcohol, or other solvents and sealed from the external atmosphere by non-soluble ring media. [88] The choice of mounting medium is crucial to preserving the stained tissue sections and ensuring high-quality imaging during light microscopy. In this study, both aqueous and organic mounting media were optimized based on the specific requirements of the sample and analysis.

Our lab-made aqueous mounting media was applied when compatibility with water-soluble stains and analytes, such as oil Red O and fats, was necessary. These media provided excellent optical clarity and minimized the risk of disrupting the stain, making them ideal for immediate imaging; however, their temporary nature and susceptibility to hardening required careful handling and prompt imaging after preparation.

Organic or anhydrous mounting media are generally permanent and, therefore, suitable for the long-term storage of stained tissue sections. [89] These media, typically polymer resin-based, offer superior stability and durability, especially for archival purposes. However, the use of organic media necessitated dehydration and clearing of the tissue sections through a series of graded ethanol and xylene steps before application. This subsection highlights the significance of selecting the appropriate mounting medium to balance immediate imaging needs and long-term preservation, ensuring the integrity of the tissue sections for both microscopy and subsequent analysis.

#### 1.4 Integrating IMS with Histologically Stained Tissue

During the development of mass spectrometry imaging, having optical reference images of adjacent stained tissues was essential, as noted by Todd et al.[90] The first serious attempts to integrate IMS and histologically stained tissues emerged in the late 1990s as researchers, including the Caprioli laboratory, explored the potential of MALDI-IMS for biological samples.[91] Early studies focused on using optical images of adjacent tissue sections stained with cresyl violet to provide structural context, while IMS was crucial for understanding the molecular distribution within the tissue.[92] Notably, a study utilizing MALDI-TOF mass spectrometry for neuropeptide analysis in fresh rat brain tissue demonstrated the integration of toluidine blue staining on consecutive sections to accurately localize anatomical regions, such as the supraoptic nucleus.[93]

Additionally, using hematoxylin and eosin-stained sections as a guide, fresh-frozen tumor sections were analyzed, revealing over 1,600 distinct protein species across 50 samples.[94] The study identified 82 discriminatory MS signals that distinguish between tumor and normal lung tissue with high accuracy. However, to perform a comprehensive chemical imaging of a tissue section, multiple analyses on consecutive tissue sections are often required per biological sample; thus, correlating multimodal data is challenging, as anatomical features can vary from one tissue section to another. [95] Hence, there is an increasing need to perform IMS and subsequent staining on a single tissue section. Significantly, Chaurand et al. demonstrated the compatibility of several wellestablished nuclear tissue staining protocols with MALDI-MS analyses of the same tissue section.[96] Previously, another group had found that hematoxylin and eosin stains severely interfered with the spectral quality obtained from the direct analysis of H&E-stained LCM cells imaged with MALDI-MS.[97] To overcome this hurdle, the matrix needed to be washed off the surface of the tissue before it was subsequently stained with H&E. This was demonstrated by Shwamboin et al., who were able to identify specific protein expression patterns for normal and cancerous regions within the prostate tissue sections using the same section for imaging followed by staining.[98] In contrast, the sample preparation step for a typical TOF-SIMS analysis is minimal and does not require the addition of a matrix to the sample before analysis. Thus, it is possible to work on the same tissue section staining with H&E before or after imaging, preferably by acquiring the TOF-SIMS images before staining, as reported by Bich et al. In this study, using a rat brain section, they demonstrated that vacuum conditions did not disturb the staining or the recognition of brain structure.[99]

Integrating IMS with traditional histology can be a time-intensive process, often requiring meticulous sample preparation and multiple procedural steps to ensure accurate results.

Technological advancements in computational tools for analyzing and visualizing combined data have been pivotal. For example, peak picking and alignment help reduce dataset size while retaining essential spectral information.[100] Numerous commercial and open-source visualization software options are available, many of which support the standardized imzML data format.[101]

Here, we explore a workflow for multimodal tissue analysis (sequential vs. consecutive) by combining MALDI and SIMS with optical imaging of histologically stained tissues, thereby enhancing the interpretative value of the samples. Furthermore, we utilized laser-etched indium tin oxide (ITO) glass slides to enhance image registration accuracy, aiming to achieve spatial resolutions capable of single-cell analysis.

#### 1.5 Challenges of Coregistering

Registration involves aligning two or more images taken from the same or different modalities so that they are overlaid on top of one another. Coregistering IMS data with optical imaging of histologically stained tissue involves various technical and methodological challenges. These issues must be carefully managed to ensure that molecular data from IMS aligns accurately with structural details from histology, enhancing meaningful biological insights.

One of the primary challenges in coregistration is the difference in spatial resolution between IMS and histological imaging. IMS data exhibits a high-dimensional nature, consisting of tens to hundreds of spectral channels, each dedicated to capturing a specific and distinct molecular distribution. In contrast, optical images of histological data typically have much lower dimensionality, often limited to single- or three-channel representations, providing a broader view of tissue patterns.[102] Consequently, accurately overlaying the two datasets can be tedious, as

molecular features visible in IMS may not correspond exactly to the structures observed in histology. Methods to overcome this often involve using landmarks, which can be extraneous marks added during sample preparation or acquisition, or unique features visible in both images. [51] However, this would only be feasible for the same tissue section workflow. Another challenge arises from the differences in sample preparation for IMS and histology, which can lead to tissue deformation or shrinkage, complicating the alignment process.[103] This is the case for the same and adjacent tissue section workflow. Histological preparation commonly involves dehydration and staining steps that can cause tissue shrinkage [16], whereas IMS often utilizes frozen or chemically treated sections, which can also shrink under vacuum conditions. [104] For example, Sangwon et al. noted a mismatch between chemical and optical images in direct profiling and imaging of plant metabolites in intact tissue.[105] Advanced computational techniques, such as nonlinear transformations, are often required to correct these deformations; however, they can add complexity to the registration process.[106] Further complicating co-registration is the issue of incompatible data formats and the need for data integration between IMS and optical imaging data of histologically stained tissues. IMS data typically uses the imzML format, consisting of a small file (text or XML) that stores all metadata (e.g. instrumental parameters, sample details), and a larger binary file holding the mass spectral data,[101] whereas histology images are more commonly stored as TIFF or JPEG files, which prioritize color and spatial detail.

Addressing these challenges is crucial for harnessing the full potential of IMS and classical histology, thereby facilitating their integration. Successfully overcoming these obstacles will improve the precision and applicability of co-registered IMS and histological data, leading to deeper insights into molecular pathology and advancing the field of disease research.

#### 1.6 Thesis Aims and Objectives

The goal of this work was to develop a workflow for integrating imaging mass spectrometry (IMS) data with optical images of histologically stained tissue, with a focus on achieving accurate single-cell level coregistration. We evaluated the limitations of using consecutive tissue sections and demonstrated that they cause misalignment at the cellular level. To address this, we implemented a same-section multimodal imaging approach combining SIMS, MALDI, and H&E staining.

A key feature of our method was the use of laser-etched fiducial markers on indium tin oxide (ITO) slides to improve the accuracy of image coregistration across different modalities. We further leveraged an open source, deep learning-based segmentation tool (CSGO) to isolate whole-cells from hematoxylin and eosin-stained mouse brain tissue images, allowing for pixel-level linkage between histological features and spatially-resolved IMS information. This work advances a framework for improved spatial alignment between histology and IMS, and for detailed subcellular molecular tissue analysis at high resolution.

#### **Chapter 2: Research Methodology**

#### 2.1 Methodology of Integration

Mouse brains were obtained from the Animal Care Facility at Concordia University, Loyola Campus. C57BL/6 mice (male and female) born in December 2022 or January 2023 were euthanized at 21 or 24 weeks of age. Whole brains were extracted, soaked in 0.9% NaCl to prevent drying, wrapped in sterile gauze, and transported on ice before storage at -80°C. The mice were euthanized for another experiment, aligning with the 3Rs principles (Reduction, Refinement, and Replacement) to maximize sample use, minimize unnecessary animal use, and ensure ethical research practices, we utilized the unmodified and unused tissues for our research. Mice brain tissues collected on either a laser-etched ITO or plain glass slide were analyzed using cluster ion beam secondary ion mass spectrometry (SIMS) and/or matrix-assisted laser desorption ionization mass spectrometry, with a 1,5-diaminonaphthalene matrix applied for high-resolution imaging. The resulting IMS images were overlaid with serial or post-analysis hematoxylin and eosin (H&E) stained sections.

1.



Figure 1 Prototype microscope slide etched using a Rayjet desktop laser engraver (Trotec) equipped with a 30W CO<sub>2</sub> laser, which features a spatial resolution of 400 μm.

Figure 1 shows a prototype microscope slide that was laser-etched using a Rayjet desktop laser engraver (Trotec) equipped with a 30-watt CO<sub>2</sub> laser. The etching process was used to generate

fiducial markers directly onto the surface of the indium tin oxide (ITO) glass slide. These markers were intended to serve as fixed spatial reference points for image coregistration across multiple imaging modalities, including histology and imaging mass spectrometry.

#### 2.1.1 Same tissue vs adjacent tissue workflow

The whole brain was partially embedded in an OCT medium, mounted on a disk, and then placed in a cryostat. Coronal mouse brain sections, 10 µm thick, were cut at -20°C. Three consecutive sections were prepared, with the first and last placed on laser-etched ITO glass slides and the second on a plain glass slide.

The first section was analyzed using cluster ion beam secondary ion mass spectrometry (SIMS), followed by the application of a 1,5-diaminonaphthalene matrix and analysis using matrix-assisted laser desorption ionization. Afterward, the matrix was washed off by dipping the slide in 90% ethanol for 1 minute, and the section was then stained with H&E before being imaged with a Nikon Eclipse Ti microscope. The second section was stained with H&E for histological analysis and optical imaging. The third section underwent MALDI analysis, followed by matrix removal and light microscopy after H&E staining. For same-tissue analysis, SIMS, MALDI, and optical images of the H&E-stained tissue were overlaid using tissue features for alignment. This was compared to adjacent-tissue analysis, where SIMS images from section 1, H&E from section 2, and MALDI images from section 3 were aligned based on shared tissue features.

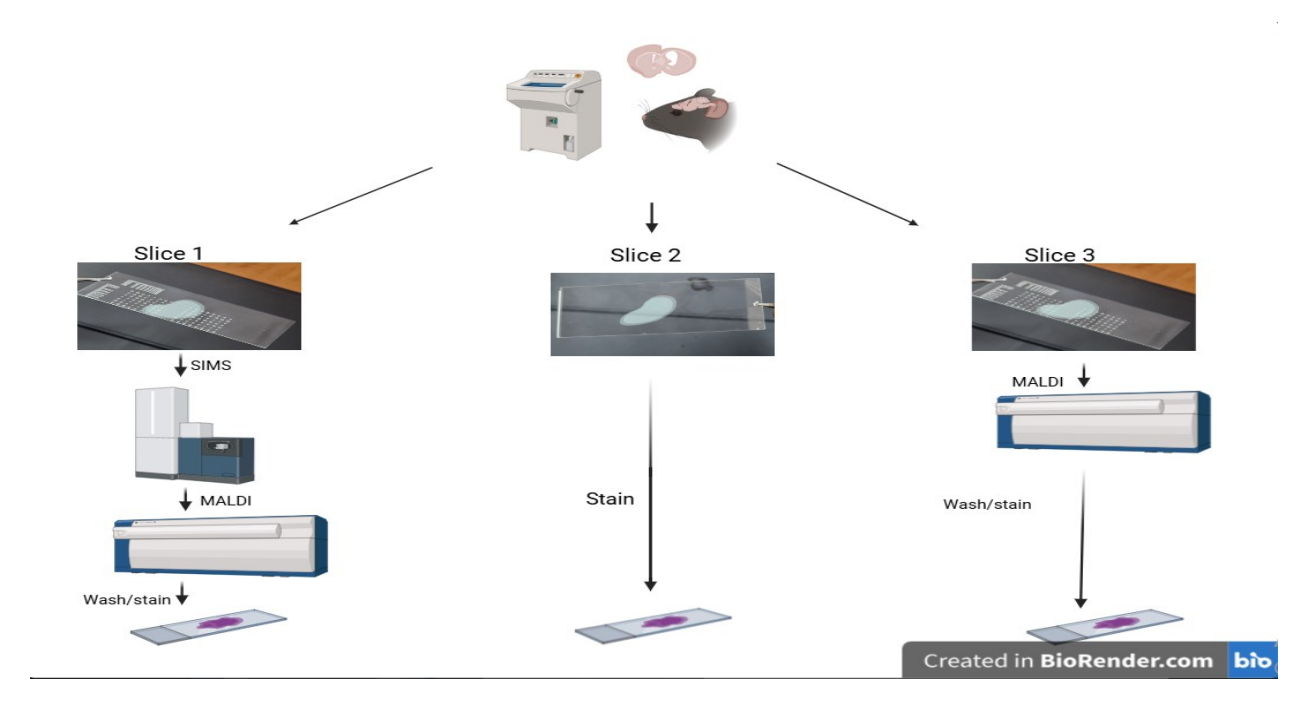


Figure 2 Schematic representation of our workflow.

**Figure 2** is a schematic of the consecutive versus sequential tissue imaging workflow. Three coronal mouse brain tissue sections were cut using a cryostat. The first and third tissue sections went on laser-etched glass slides, while the second was on a plain glass slide. The first section was imaged sequentially. It was first analyzed with TOF-SIMS and then with MALDI-TOF. After this, the matrix was washed away before H&E staining. The second section, on a plain glass slide, was stained with H&E for histological reference. The third section underwent MALDI-TOF imaging, followed by matrix removal and H&E staining. This workflow facilitates the integration of multimodal imaging techniques while maintaining histological integrity, allowing for both molecular and morphological analysis of the same and adjacent tissue regions.

#### 2.1.2 Laser-etched fiducial markers for co-registrations

The first tissue slice was collected on a laser-etched indium tin oxide (ITO) glass slide. The tissue section was analyzed using cluster ion beam secondary ion mass spectrometry (SIMS). A 1,5-diaminonaphthalene (DAN) matrix was then applied for analysis with matrix-assisted laser desorption ionization (MALDI). Following this, the matrix was removed by immersing the slide in 90% ethanol for 1 minute. The tissue section was subsequently stained with H&E, coverslipped, and optically imaged using a Nikon Eclipse Ti microscope. We coregistered H&E-stained multimodal IMS tissue section with a consecutive H&E-stained section (10 µm apart) using visible tissue features. While this achieved general alignment, we observed mismatches at the single-cell level, revealing limitations in relying solely on anatomical features and/or different tissue sections. Afterwards, we coregistered the multimodal data from the same tissue section using laser-etched fiducial markers, which enabled precise alignment down to individual cells and significantly improved the accuracy of subsequent molecular analyses.

#### 2.2 Secondary ion mass spectrometry (SIMS) Analysis

SIMS IMS is a surface analysis technique capable of producing high-resolution chemical images and is a well-suited platform for analyzing lipids directly from the surface of biological materials.[107] Unlike MALDI, SIMS uses primary ions (*e.g.*, Ar+, Ga+, In+) to strike the sample surface [108], making it particularly well-suited for analyzing fine structural and compositional details at the subcellular level. This study utilized SIMS to map molecular distributions within tissue sections, allowing for precise co-registration with histological and MALDI imaging data. This section describes the use of a primary ion beam, selected for its ability to produce high-quality molecular data while preserving tissue integrity. Sample preparation was optimized to minimize

contamination and ensure quality data acquisition. Critical parameters, such as beam energy, ion dose, and raster size, were tailored to maximize beam current while maintaining high spatial resolution.

#### 2.2.1 Instrumentation and parameters

Time-of-flight Secondary Ion Mass Spectrometry (SIMS) analysis was conducted at the Département de génie physique, Polytechnique Montréal, Montréal, QC, Canada. The measurements were performed using an ION-TOF SIMS IV instrument (IONTOF GmbH, Germany) with a bismuth cluster ion source (Bi<sub>3</sub>+). The system operated at an acceleration energy of 25 kV with a primary ion current of 1 pA, employing bunched mode for enhanced mass resolution and a pulse width of 29.7 ns.

Analyses were conducted in static mode, ensuring the primary ion dose remained below  $5 \times 10^{10}$  ions/cm² to minimize surface damage. The maximum analyzed depth was approximately 10 Å. Throughout the experiment, the vacuum chamber pressure was maintained at  $5.0 \times 10^{-9}$  Torr. To prevent surface charging, charge compensation was applied using an electron flood gun operating at 2.4 A. Spectral data were acquired over a 500  $\mu$ m  $\times$  500  $\mu$ m area with a resolution of 64  $\times$  64 pixels. Additionally, large-area ion images were collected in stage raster mode across a 7000 mm  $\times$  11000 mm surface at a resolution of 896  $\times$  1408 pixels.

#### 2.3 Matrix-assisted laser desorption ionization (MALDI) Analysis

MALDI IMS is a label-free, tissue-based throughput analytical technology for the qualitative and quantitative spatial analysis of biomolecules, including proteins and peptides, lipids, drug molecules, and their metabolites.[109] MALDI IMS utilizes a laser to desorb and ionize analytes mixed with the matrix molecule, facilitating the desorption and ionization process. [110] In this

study, MALDI was employed to provide complementary insights into histologically stained tissues by combining it with SIMS imaging. The section outlines the procedures involved in MALDI analysis, focusing on matrix application, instrument settings, and parameters to ensure the acquisition of viable data.

The workflow started by carefully preparing frozen tissue samples to ensure compatibility with MALDI, followed by the application of a suitable matrix, which plays a crucial role in ionization efficiency and lateral resolution.[111] Instrument parameters, such as laser energy and resolution, were optimized to achieve high-quality data. Through this approach, MALDI imaging provided detailed molecular profiles that were coregistered with SIMS and optical images of histologically stained tissues, enabling a comprehensive analysis of the tissue samples.

#### 2.3.1 Matrix deposition

Matrix deposition was performed using a sublimation apparatus. The laser-etched indium tin oxide (ITO) slide was taped to the bottom of the condenser. The condenser was filled with ice water to maintain a temperature of approximately 0 °C. The sublimation bell was under a vacuum for 5 minutes before being filled with silicon oil to heat it, thereby stabilizing the conditions. After being placed in the oil, 1,5-diaminonaphthalene (DAN) was allowed to sublimate for 7 minutes. The sublimation bell was then removed from the oil, and the ice was removed from the condenser. The slide was allowed to equilibrate to room temperature before removing it from the vacuum. Matrix density was calculated by weighing the slide before and after sublimation.

#### 2.3.2 Instrumentation and parameters

The sample was imaged at the Université de Montréal in Professor Pierre Chaurand's laboratory using a Bruker MALDI TOF/TOF Ultraflextreme instrument equipped with a Smartbeam laser operating at a frequency of 1000 Hz. Spectra were acquired at a 35 µm lateral resolution using a

reflectron geometry in positive ion mode, targeting the 640-960 Da mass range, which is relevant to phospholipids. Laser fluence and delayed extraction parameters were optimized for maximum sensitivity and mass-resolving power. Imaging data was processed using FlexImaging and exported as an imzML file.

#### 2.4 Hematoxylin and Eosin Staining

Histological staining and light microscopy are cornerstone techniques in tissue analysis, providing detailed, high-resolution morphological context to molecular imaging data. Histological staining is the gold standard for tissue examination in clinical pathology and life-science research, as it visualizes tissue and cellular structures using chromatic dyes or fluorescence labels to aid in the microscopic assessment of tissue.[112] While we have various types of staining, hematoxylin and eosin is the most widely used histological stain.[113] In a typical tissue, hematoxylin stains the nuclei blue, whereas the cytoplasm and extracellular matrix have varying degrees of pink staining with eosin.[114]

The following H&E staining protocol was adopted as a standard protocol.[115] Thaw-mounted tissue sections were hydrated by immersing the slides in a series of ethanol (C<sub>2</sub>H<sub>5</sub>OH) solutions with increasing water content. The slides were left in 100% C<sub>2</sub>H<sub>5</sub>OH (2 times), 90% C<sub>2</sub>H<sub>5</sub>OH, and 70% C<sub>2</sub>H<sub>5</sub>OH for 1 minute each, after which the tissue was rapidly rinsed (10 seconds) under running deionized H<sub>2</sub>O. The re-hydrated tissue was stained in a fresh Hematoxylin solution for 1.5 min to convert the soluble red Hematoxylin to an insoluble blue, a process known as bluing, the Hematoxylin-stained tissue sections were treated with a 0.2% ammonia solution (CAS 1525-1-29). The slide was subsequently rinsed in 90%- C<sub>2</sub>H<sub>5</sub>OH for 30 s and then stained with an Eosin solution for 60 s. The sections were dehydrated in a series of ethanol solutions, 90% C<sub>2</sub>H<sub>5</sub>OH,

100% C<sub>2</sub>H<sub>5</sub>OH, and 100% C<sub>2</sub>H<sub>5</sub>OH, for 60 s, 30 s, and 30 s, respectively. Finally, the sections were cleared in two consecutive xylene solutions for 60 seconds. A coverslip was added using an SP15-100 permount mounting medium (obtained from Fisher Scientific, Canada).

3a.

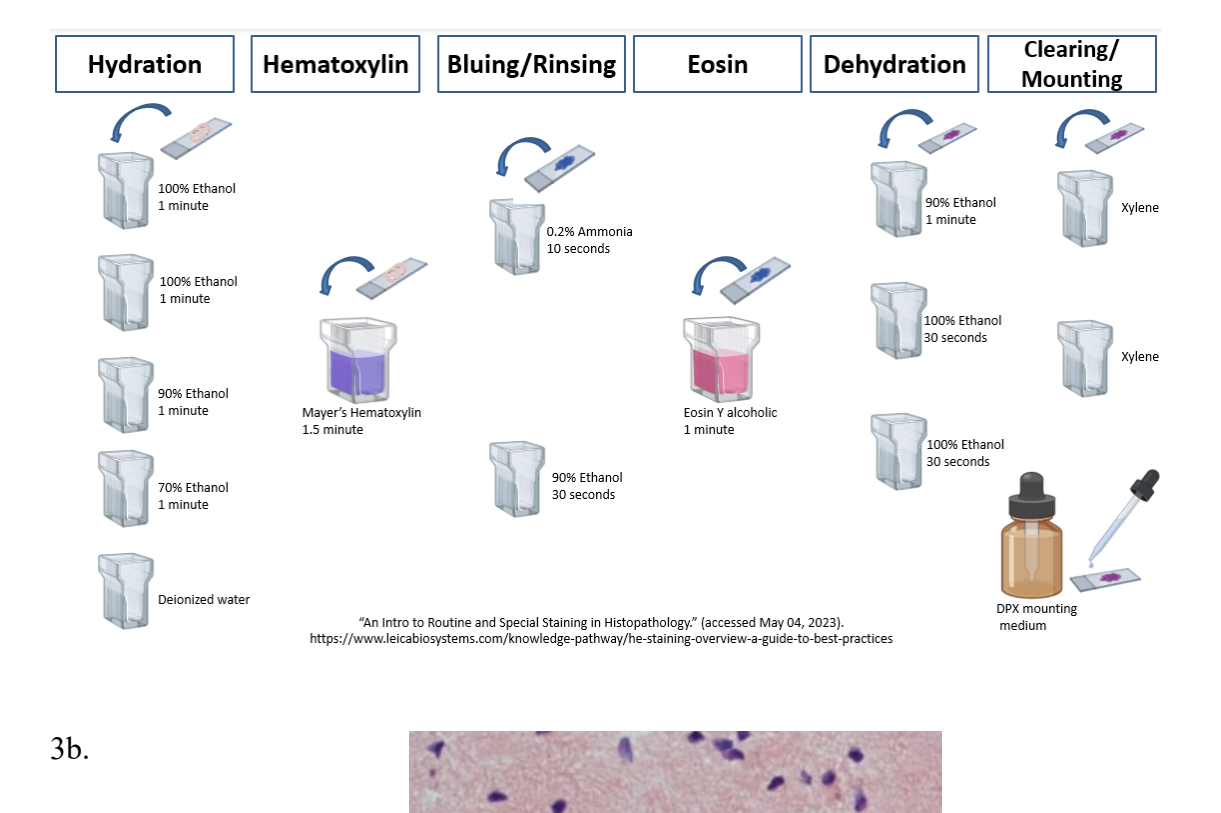


**Figure 3.a)** Modified H&E staining protocol and **b)** H&E-stained optical image of the hippocampus region of mouse brain tissue (scale bar =  $50 \mu m$ ).

**Figure 3a** presents a schematic representation of the modified H&E staining protocol. The process begins with hydration to reintroduce moisture into the tissue, followed by hematoxylin staining to visualize nuclei. A bluing and rinsing step ensures the conversion of the initial red-purple hematoxylin stain to a deeper blue color. Eosin staining is then applied to highlight cytoplasmic structures. The protocol concludes with dehydration and clearing to maintain tissue morphology before final mounting. This optimized workflow enhances stain consistency and tissue integrity for improved histological analysis. **Figure 3b** is the hippocampus region of a mouse brain that has been stained using our modified hematoxylin and eosin staining protocol.

#### 2.4.1 Light Microscopy

Brightfield images of H&E- and oil red O-stained tissues were captured using a Nikon Eclipse Ti microscope equipped with a Nikon DSRi2 camera (3x3 binning, pixel size 0.88 μm) and a 20x (NA 0.75) or 10x (NA 0.45) plan APO dry objective lens, with no further magnification. Each tissue section needed to be scanned twice at different focal lengths to obtain an even focus across the large surface area.

## Chapter 3: Results

The accuracy and reliability of combining Imaging Mass Spectrometry (IMS) and histology data relies on effective data processing techniques. This chapter outlines the key steps in processing, overlaying, and analyzing our image datasets. This process begins with image preprocessing, followed by advanced segmentation techniques and statistical analysis to extract meaningful biological features using software like the R programming language, Python, and MATLAB. Additionally, coregistration methods using traditional tissue features as well as our laser-etched fiducial markers were applied to align and merge data from multiple modalities with different resolutions, ensuring precise spatial correlation.

### 3.1 Data Formats

Imaging Mass Spectrometry (IMS) and histology experiments provide various types of image data, each offering unique insights into tissue morphology and molecular distribution. A common challenge in dealing with IMS data is that IMS vendors provide proprietary software for data processing and visualization that is incompatible with data from other manufacturers.[116] Analyzing IMS data becomes even more complicated due to the very large size of imaging datasets and the reporting of numerous data routines, coupled with insufficient training and inadequate review.[117] IMS experiments can produce extremely large datasets; for example, a 4 cm × 4 cm MALDI target plate imaged at a pixel size of 100 μm × 100 μm results in 160,000 pixels. If we assume 100 kB per spectrum (6400 m/z bins), then the dataset would be approximately 15.26 GB.[118] The standard data format for Imaging Mass Spectrometry data is called imzML (Imaging Mass Spectrometry Markup Language)[119], which is an XML-based format designed to efficiently store and exchange large mass spectrometry imaging datasets across different instruments and analysis software; it is essentially a modified version of the broader mzML format

for general mass spectrometry data.[120] However, our Time-of-Flight Secondary Ion Mass Spectrometry (TOF-SIMS) analysis data were stored in BIF6 format. A ".bif6" file is a specialized binary format used in ToF-SIMS data storage; these files serve as containers for preprocessed mass spectrometry data collected from scientific instruments.[121] Regardless of differences in formats, by processing our IMS data, we can generate intensity maps where pixel intensity corresponds to ion abundance. On the other hand, brightfield images of H&E- and oil red O-stained tissues, captured using a Nikon Eclipse Ti microscope as highlighted in Chapter 2, were stored in ND2 format and exported as TIFF data directly from the instrument for easier readability in MATLAB.

# 3.2 Image Processing using R programming language

R is a free, open-source programming language for statistical computing and data visualization.[122] Considering the difficulty of directly reading the imzML format into the MATLAB workspace, we have adopted R. Using the Cardinal package in R, we processed our Time-of-flight Matrix-Assisted Laser Desorption Ionization data in the imzML format. Cardinal is an R package for the statistical analysis of mass spectrometry-based imaging experiments of biological samples such as tissues.[123]

We used the "readMSIData" function to read our TOF-MALDI data into the R environment. This dataset was preprocessed by normalizing to the total ion current to ensure that all mass spectra in the set are comparable to each other. Furthermore, we visualized and picked the ion image of lipid galactosylceramide for further image processing in MATLAB; one of the ion images with unique and distinct feature in the tissue, making it suitable for feature-based co-registration. To preserve the quality of our selected ion image, we exported the xy coordinates along with their intensity values as a CSV file to be reconstructed in MATLAB.

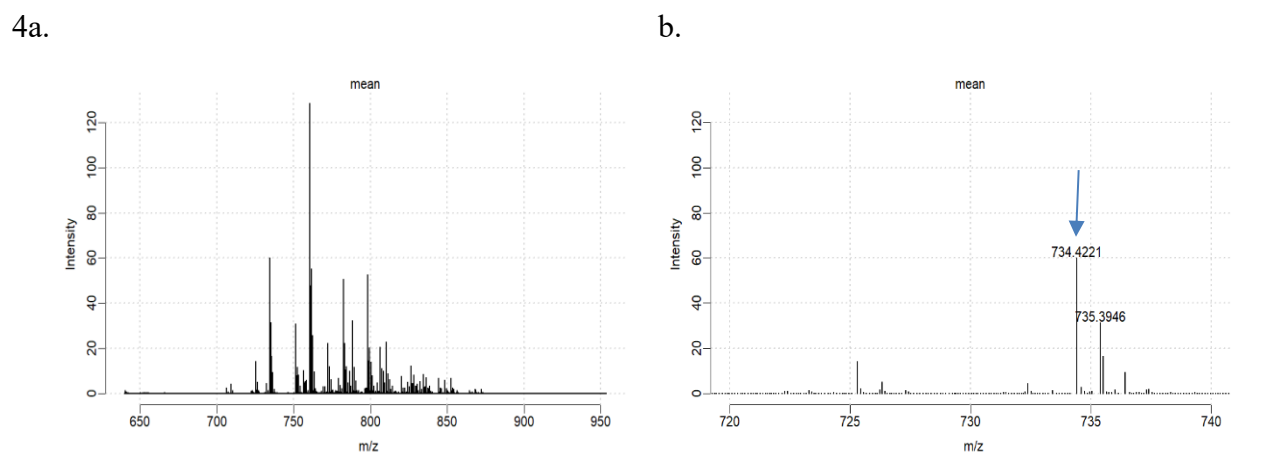


**Figure 4.a)** Mean spectra of Multimodal IMS mouse brain tissue section 1 and **b)** zoomed in spectra highlighting lipid peak dipalmitoyl phosphatidylcholine (DPPC) with the blue arrow

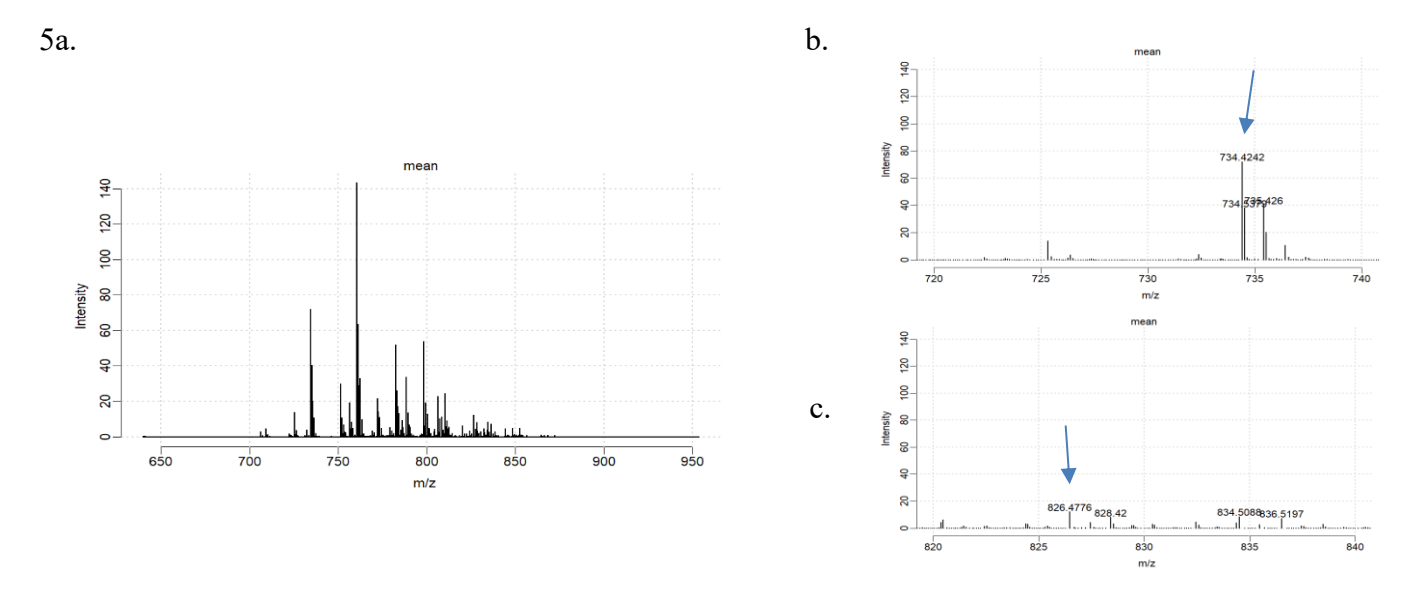


**Figure 5. a)** MALDI-ToF mean spectrum of mouse brain tissue section 3, **b)** zoomed view highlighting dipalmitoyl phosphatidylcholine (DPPC), and c) zoomed view highlighting galactosylceramide (GalCer), both indicated by blue arrows.

**Figures 4** and **5** illustrate the mean spectra of mouse brain tissue (Sections 1 and 3) analyzed using the MALDI TOF/TOF Ultraflex, equipped with a smartbeam laser operating at 1000 Hz. In **Figures 4a** and **5b**, the spectra have been preprocessed by normalizing to the total ion current. The

highlighted peaks at *m/z* 826 and *m/z* 734 correspond to the lipids galactosylceramide (Galcer) and dipalmitoyl phosphatidylcholine (DPPC), respectively.

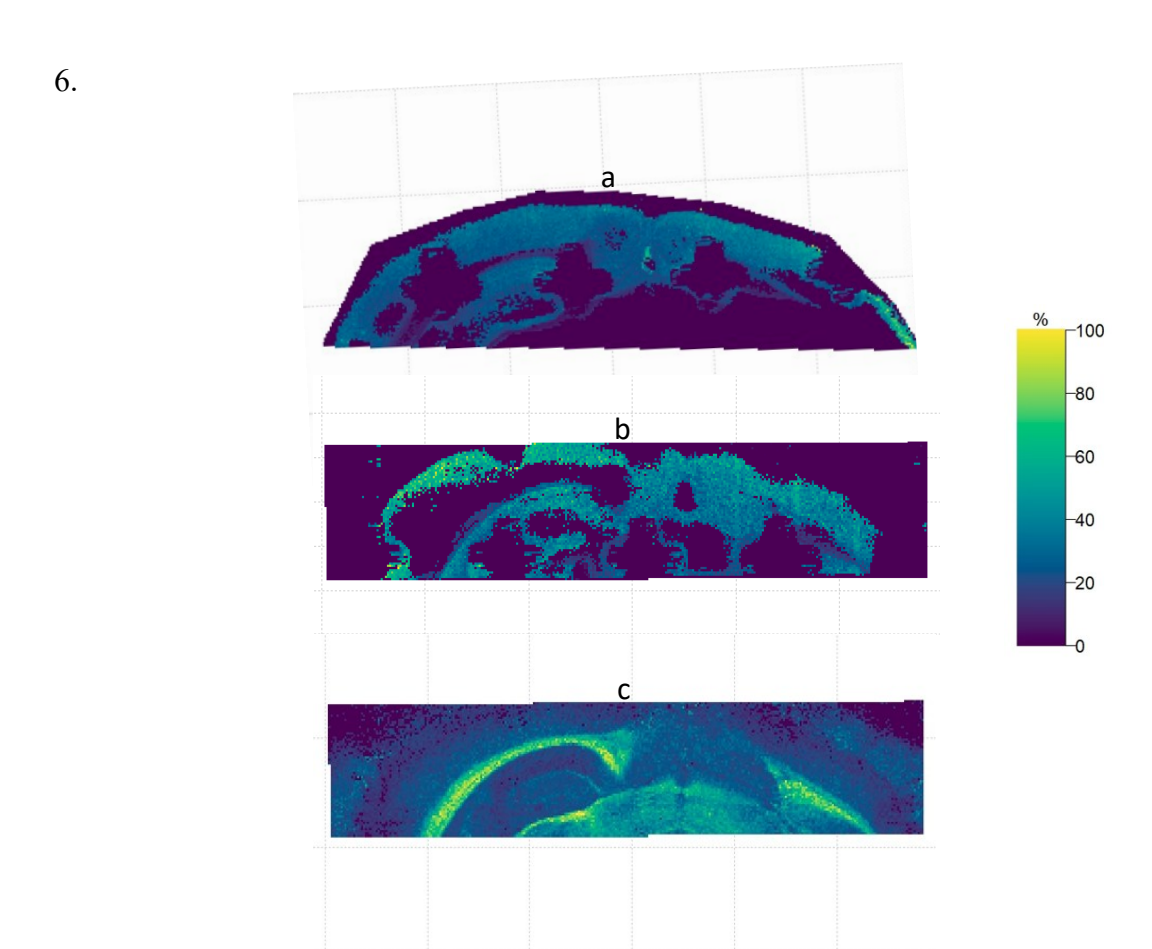


Figure 6.a) MALDI-ToF ion image of DPPC (m/z 734) in multimodal IMS mouse brain tissue section 1, b) DPPC ion image in mouse brain tissue section 3, and c) GalCer (m/z 826) ion image in mouse brain tissue section 3.

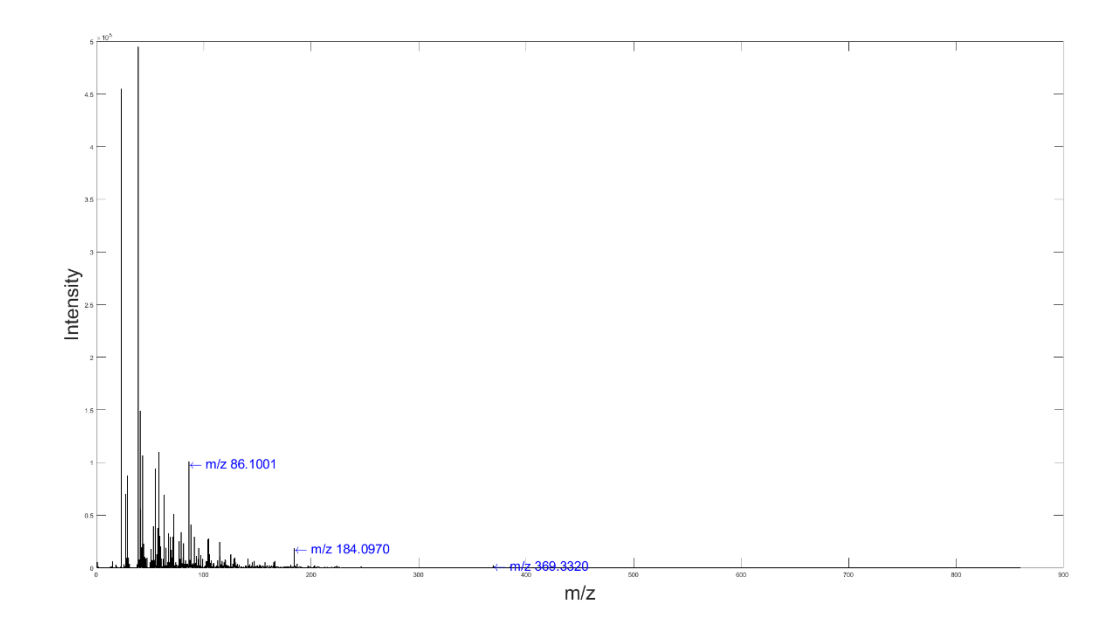
**Figure 6** shows ion images of selected lipids. **Panel 6a** displays the spatial distribution of DPPC (m/z 734) in tissue section 1. **Panel 6b** shows the distribution of DPPC (m/z 734) in tissue section 3. Meanwhile, **Panel 6c** depicts the distribution of GalCer (m/z 826) in tissue section 3. The color

scale represents ion intensity as a percentage of the maximum signal observed for each respective image, allowing for relative comparison of ion abundance. In **panels 6a**, **6b**, and **6c**, the maximum observed ion intensity is 150, which corresponds to 100% on the normalized color scale.

## 3.3 Image Processing using MATLAB

MATLAB stands for Matrix Laboratory.[124] Designed by Cleve Moler and developed by MathWorks Inc. (Massachusetts, USA), it is a versatile programming language primarily used for numerical computation.[125] MATLAB provides a powerful environment for image processing, offering a range of built-in functions and toolboxes designed for tasks such as image enhancement, segmentation, filtering, and transformation. Further analyzing the MALDI-ToF preprocessed data, we wrote custom code in MATLAB to reconstruct our exported CSV file as an image. Here, we read our ToF-SIMS dataset in "BIF6" format directly into our workspace using the built-in "fopen" function.

7a.



7b.

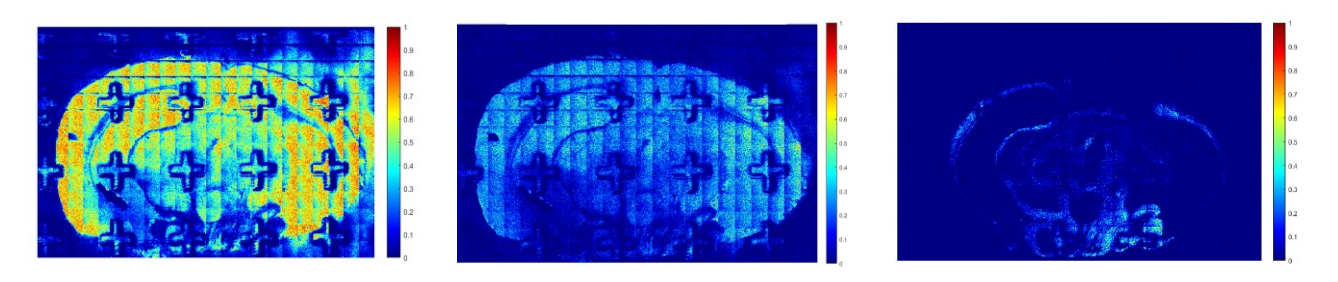


Figure 7.a) ToF-SIMS mean spectra from multimodal IMS mouse brain tissue section 1, with annotated fragments: m/z 86 and 184 (phosphocholine head group) and m/z 369 (cholesterol); b) corresponding ion images for m/z 86, 184, and 369 (left to right), illustrating their spatial distribution within the tissue.

Figure 7a presents the mean spectra of the TOF-SIMS dataset for tissue section 1, showing the averaged mass spectra data from multiple points across the tissue section. The m/z 184 ion, which corresponds to the phosphocholine head group, is highlighted to show its presence in the tissue.

From left to right, **Figure 7b** displays the ion image of fragments phosphocholine head group (PC, m/z = 86, m/z = 184) and cholesterol (m/z = 369), illustrating their spatial distribution across the tissue section. The phosphocholine-related fragments (m/z = 86 and m/z = 184) exhibit strong and widespread co-localization throughout the gray matter, with particularly intense signals in the cortical and hippocampal regions. In contrast, the cholesterol fragment (m/z = 369) displays a more localized and distinct distribution, with higher intensities observed in white matter regions and subcortical structures. Overall, the ion images show the localization of various chemicals, providing insights into molecular heterogeneity and enabling correlations with other imaging modalities for more comprehensive tissue analysis.

## 3.4 Image Registration

Image registration is the process that performs spatial transformation and aligns a set of images to a common observational frame of reference, typically a chosen image from the set.[126] The primary goal of an image registration algorithm is to transform a source image geometrically so that it is spatially or temporally aligned with a reference image.[127] This process maps points from space X in one view to space Y in another, where the transformation T applied to a point x in X generates a transformed point  $x^i$ .[128]

# **Equation 1.** Fixed point equation

$$x^i = T(x)$$

Some common types of geometric transformations include affine, rigid, non-rigid, and projective transformation.

Using the "flipIr" function, MALDI-TOF ion images were all flipped to have the same orientation as our TOF-SIMS ion image, enabling a better image overlay. Subsequently, we adopted the "cpselect" function, a Control Point Selection Tool, which is a graphical user interface that enables the selection of control points in two related images: a fixed or reference image and a moving image. This tool opens a graphical user interface (GUI) that allows you to manually select and save the x and y coordinates of the same points on both our fixed and moving images. Furthermore, we used the "Fitgeotform2d" function to transform the saved coordinates projectively. This is the most general geometric transformation. Here, two 2D points p' and p (represented in homogeneous coordinates) are related by a 3x3 non-singular transformation matrix (homography).[129] This is mathematically represented in equations 2 and 3 below.

## **Equation 2.** Homography equation

$$p^i = hp$$

**Equation 3.** Homography equation (standard form)

$$\begin{bmatrix} x^i \\ y^i \\ 1 \end{bmatrix} = \begin{bmatrix} h_{11} & h_{12} & h_{13} \\ h_{21} & h_{22} & h_{23} \\ h_{31} & h_{32} & 1 \end{bmatrix} \begin{bmatrix} x \\ y \\ 1 \end{bmatrix}$$

Finally, we use the "imwarp" function to align the transformed coordinates with the fixed image.

The "imshowpair" function then overlays the transformed coordinates onto the fixed (reference) image for visualization.

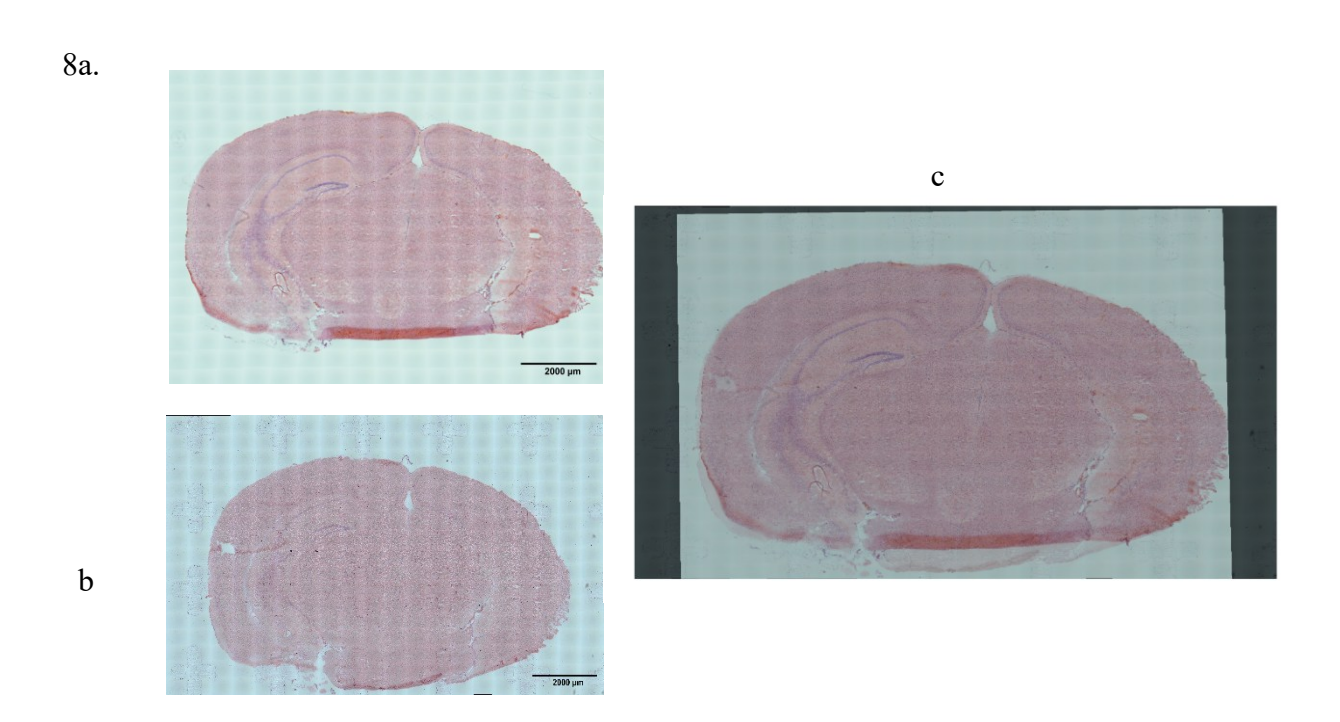
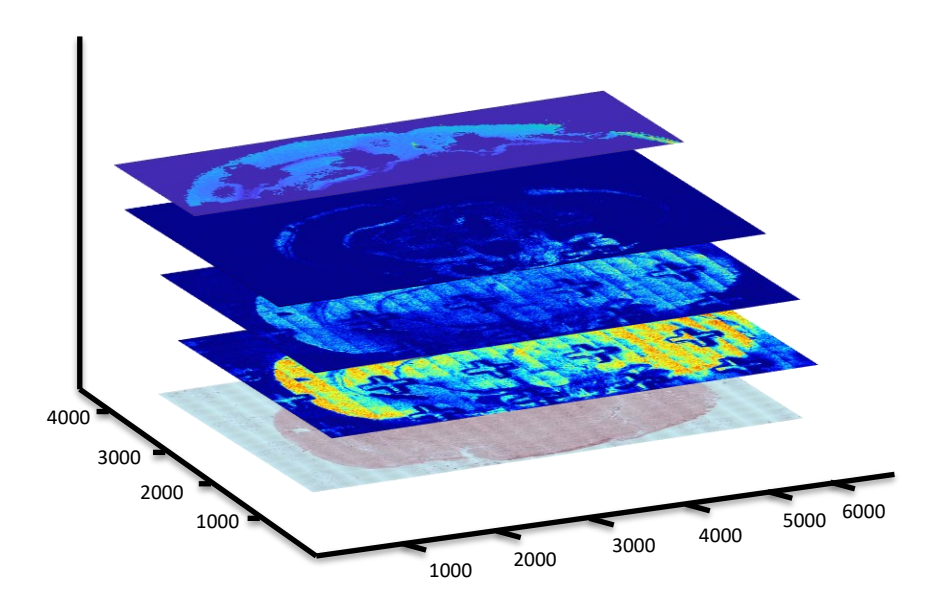


Figure 8.a) H&E-stained mouse brain tissue section 2, b) H&E-stained multimodal IMS mouse brain tissue section 1, and c) registered H&E-stained mouse brain tissue section 2 overlayed onto H&E-stained multimodal IMS mouse brain tissue section 1.

**Figure 8a** and **8b** show H&E-stained images of mouse brain tissue. **Figure 8a** depicts tissue section 2, which was stained directly after slicing, while **Figure 8b** shows section 1, stained after undergoing multimodal IMS analysis. **Figure 8c** presents the overlay of section 2 (Figure 8a) registered onto the spatial coordinates of section 1 (Figure 8b) using intrinsic features on the tissue for alignment.

9.



**Figure 9.** Same-tissue coregistration of ion images for phosphocholine fragments (m/z 86 and 184), cholesterol (m/z 369), and DPPC (m/z 734) onto the coordinates of the H&E-stained multimodal IMS mouse brain tissue section 1.

**Figure 9** illustrates the coregistration of ion images acquired from both ToF-SIMS and MALDI-ToF imaging experiments onto the spatial coordinates of the H&E-stained multimodal IMS tissue section 1. Specifically, the ToF-SIMS ion images correspond to m/z 86, m/z 184, and m/z 369, while the MALDI-ToF image corresponds to m/z 734. These ion distributions were geometrically aligned with the optical image of the same tissue section using traditional tissue features as well as fiducial markers etched onto the glass slide, enabling precise overlay of molecular signals onto histological structure.

## 3.4.1 Jaccard Similarity

To evaluate the accuracy of the consecutive tissue image overlay presented in **Figure 8**, especially given that both sections underwent different processing workflows, a numerical assessment was necessary. Such evaluation was also essential to assess same-tissue versus consecutive-tissue image coregistration for single-cell IMS analyses. We adopted Jaccard similarity as a tool to rate the performance of our image registrations. Jaccard similarity, also known as the Jaccard index, is a statistic that measures the similarity between two data sets. It is measured as the size of the intersection of two sets divided by the size of the union.[130]

## Equation 4. Jaccard Index

$$J(A,B) = \frac{|A \cap B|}{|A \cup B|}$$

Where  $|A\Pi B|$  Gives the number of members shared between both sets and |AUB| Gives the total number of members in both sets. The Jaccard similarity will be 1 if the sets are identical and 0 if they have no similarity.[131] We utilized MATLAB's "Jaccard" function to compute the similarity between our image datasets. Firstly, both images were preprocessed by color deconvolution to extract their hematoxylin channel, which corresponds to the nuclei. This was followed by cleaning up and then threshold segmenting. Finally, the Jaccard similarity between the images was computed. This is shown in Figure 10 below.

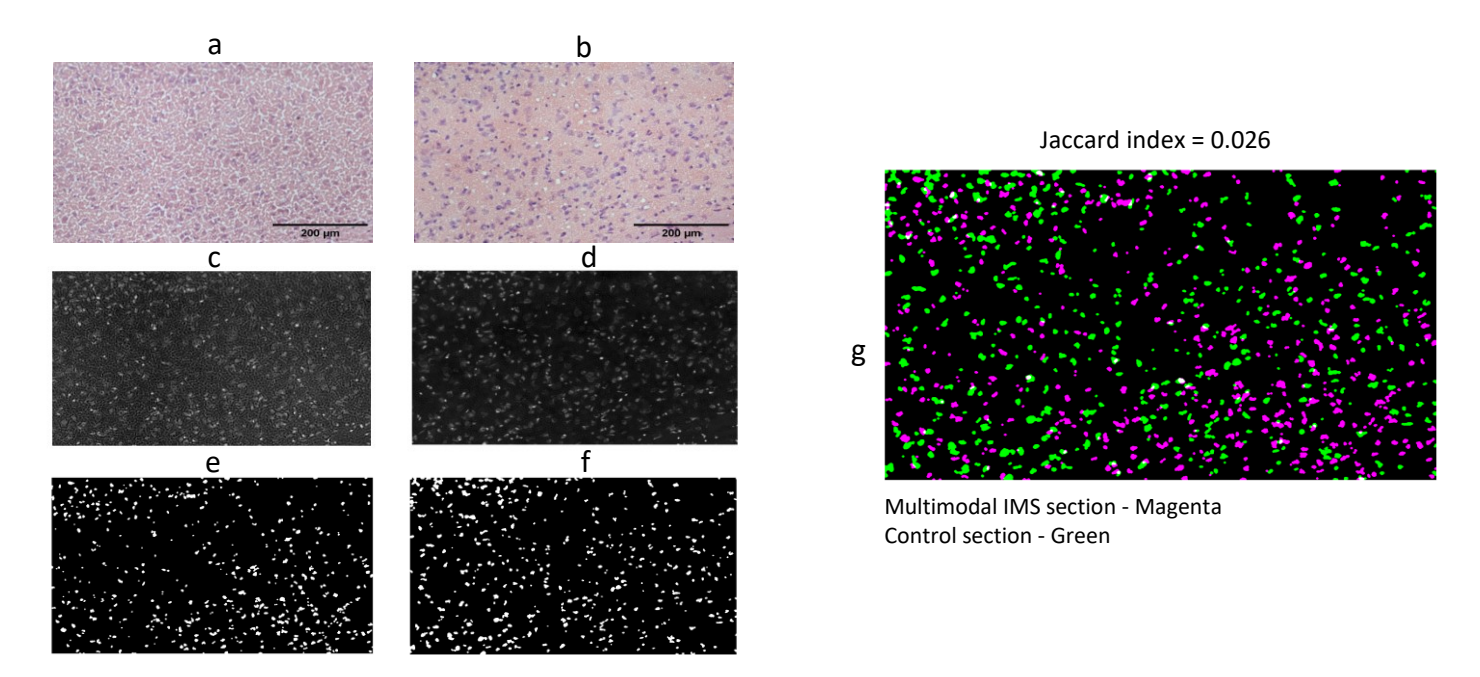


**Figure 10.** a) H&E-stained multimodal IMS mouse brain tissue section 1, b) H&E-stained mouse brain tissue section 2, c-d) color deconvolution of sections 1 and 2, respectively, e-f) threshold-segmented hematoxylin channels from sections 1 and 2, respectively, and g) overlay of the segmented masks from both sections

Figure 10 presents image processing steps and Jaccard outcomes between the H&E-stained multimodal IMS tissue section and the registered consecutive section 2. Figures 10a and 10b show the original H&E-stained images of the multimodal IMS tissue and the registered section 2, respectively. Figures 10c and 10d depict the hematoxylin channels obtained through color deconvolution of the images in 10a and 10b, respectively, highlighting nuclear features. Figures 10e and 10f illustrate the results of threshold-based segmentation applied to the hematoxylin channels of the respective sections, isolating nuclei for comparison. Figure 10g shows the overlay of the processed binary masks from 10e and 10f, with a calculated Jaccard similarity index of 0.026, indicating minimal overlap and highlighting the limitations of consecutive-section

registration for accurate single-cell IMS analysis. This low overlap emphasizes the major challenges of aligning consecutive sections for accurate single-cell IMS analysis. Although consecutive tissue slices (10 µm apart) may look similar macroscopically, they often differ at the cellular level. Moreover, small variations in cutting depth can lead to one section fully capturing a nucleus while the adjacent section only contains a partial or absent representation of the same structure. Furthermore, preprocessing steps like sectioning, mounting, and staining can cause physical distortions such as stretching, folding, or tearing, which further impair accurate cell-to-cell or pixel-to-pixel correspondence. Additionally, one of the tissue sections was analyzed using IMS, where vacuum conditions and laser or ion beam exposure can create artifacts like tissue shrinkage, matrix delocalization, and so on. These artifacts further reduce morphological integrity and registration accuracy. Overall, these findings highlight the limitations of using consecutive sections for high-resolution, single-cell multimodal IMS integration, and they stress the importance of same-section imaging approaches when aiming for single-cell molecular mapping.

## 3.5 Single-cell Segmentation

Cell segmentation is a fundamental histology imaging technique involving identifying and isolating individual cells within microscope images.[132] This process is crucial for understanding cellular behavior and disease mechanisms and developing therapeutic interventions.[133] However, segmenting cells and nuclei in 2D images of tissue samples is challenging because of their complex morphology, ambiguous overlaps, and heterogeneity in the spatial distribution of nucleus and cell membrane markers within each cell.[134] Several image segmentation techniques exist, which partition the image into several parts based on certain image features, such as pixel intensity value, color, texture, etc.[135] A few of those commonly used segmentation techniques in histopathology include Thresholding, Clustering, Active Contour Model, Level Set, and

Watershed Algorithm.[136] The aforementioned techniques would be regarded as unsupervised segmentation methods, using the intrinsic features of images for segmenting regions as noted above. On the other hand, supervised segmentation methods use deep learning models trained on labeled datasets of cell images to identify and segregate individual cells in Hematoxylin and Eosinstained tissue images. This approach relies on having a "ground truth" - manually segmented images that serve as the training data for the model.[137] For example, deep learning algorithms like convolutional neural networks (CNNs) have attracted considerable interest over the years.[138] While both approaches have their pros and cons, supervised deep-learning-based models have been shown to achieve highly accurate segmentation.[139]

In this study, segmentation was performed on H&E-stained tissue images to isolate individual cells, enabling the extraction of cell-specific molecular data from co-registered SIMS and MALDI ion images. Both unsupervised and supervised segmentation approaches were explored. Initially, unsupervised methods, such as thresholding and superpixel segmentation, were applied for this purpose. However, due to challenges such as over-segmentation, degradation from vacuum conditions, artifact formations, and poor boundary definition in crowded regions, we later adopted a supervised deep learning-based model for better single-cell delineation. Training a supervised machine learning algorithm for this task would be quite time-consuming and costly. Therefore, we used Cell Segmentation with Globally Optimized Boundaries (CSGO),[140] an open-source, already trained deep learning pipeline designed for whole-cell segmentation of hematoxylin and eosin-stained tissues. CSGO includes two components for segmentation: (1) HD-YOLO, an object detection model for localizing nuclei, and (2) U-Net, a convolutional neural network that segments membranes. These model predictions are combined with an energy-based watershed algorithm, where the nuclei serve as seed points, and the membrane boundaries define the watershed basins,

which yields an accurate individual cell mask. Distance transforms and peak detection are applied as postprocessing to improve the segmentation and recovery of any missing nuclei. CSGO outperformed existing tools, including Cellpose, on a variety of cancer tissue datasets, and is available as a web interface for ease of reproducibility.

A predefined region of multimodal IMS H&E-stained tissue and registered ToF-SIMS ion images (m/z = 86, m/z = 184, m/z = 369) was cropped for analysis. In Python, using CSGO, we whole-cell segmented the cropped multimodal IMS H&E-stained tissue into watershed regions. The resulting segmented image was then imported into MATLAB as a matrix, where the "boundarymask" function was applied to generate a binary mask outlining the perimeter of each segmented cell region. This boundary mask overlaid onto the corresponding cropped region of the co-registered ToF-SIMS ion images to ensure accurate spatial alignment between cellular structures and molecular data. Using the overlaid mask, pixel intensity values for each ion species (m/z = 86, 184, and 369) were extracted from within each segmented cell. These values were then compiled to construct individual mass spectra for each cell, enabling cell-specific molecular profiling across the selected region.

11.

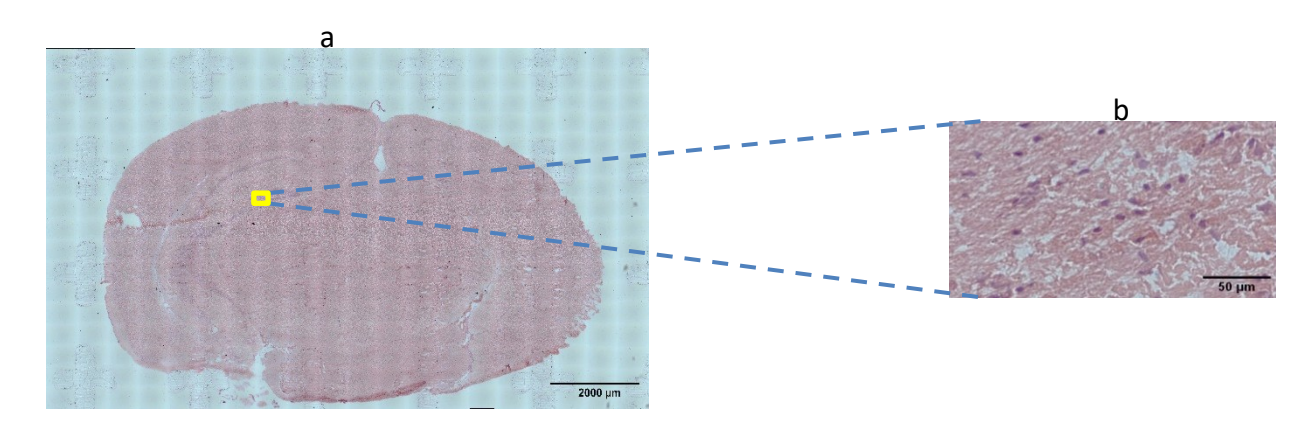
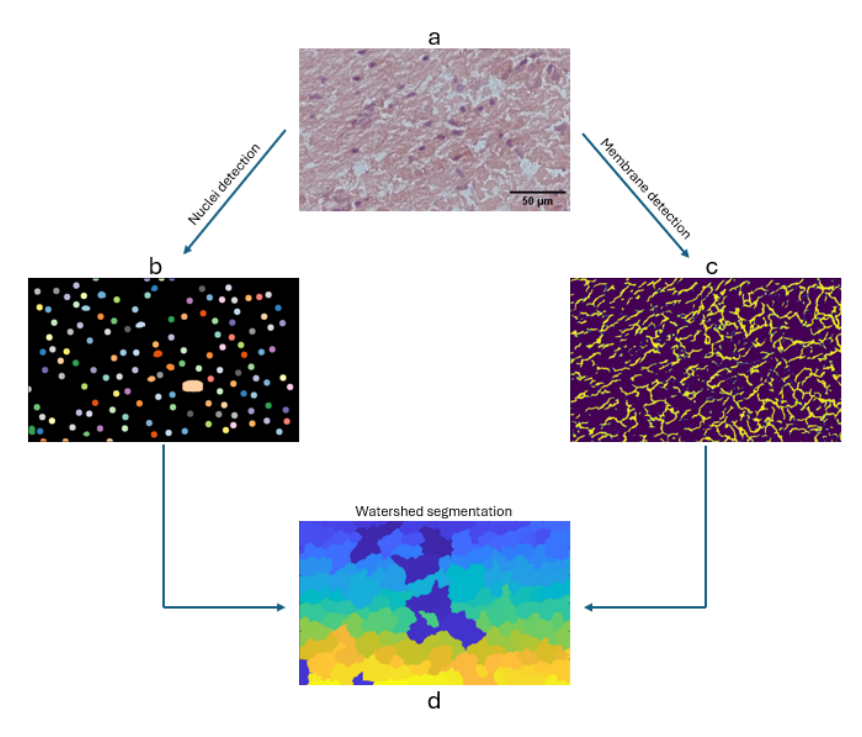


Figure 11.a) H&E-stained multimodal IMS mouse brain tissue section 1, b) cropped region from (a) highlighting the area of interest.

Figure 11a displays Hematoxylin and Eosin-stained multimodal IMS tissue section 1. Figure 11b presents a cropped region from Figure 11a.

12.



**Figure 12.a)** Cropped H&E-stained multimodal IMS mouse brain tissue section 1, **b)** nuclei segmentation, **c)** membrane segmentation of the cropped region, and d) final watershed-segmented result.

Figure 12 outlines the step-by-step whole-cell segmentation process using the CSGO (Cell Segmentation with Globally Optimized boundaries) model. Figure 12a shows the cropped Hematoxylin and Eosin-stained image from the multimodal IMS tissue section selected for segmentation. Figure 12b illustrates the nuclei probability map predicted by the deep learning model, highlighting regions with high nuclear likelihood. Figure 12c shows the corresponding cell membrane probability map, capturing the predicted boundaries between adjacent cells. Finally,

**Figure 12d** presents the watershed-segmented output, in which both nuclear and membrane predictions were integrated to generate discrete cell regions. This result represents the whole-cell segmentation used in downstream boundary mask generation and ion image overlay.

13.

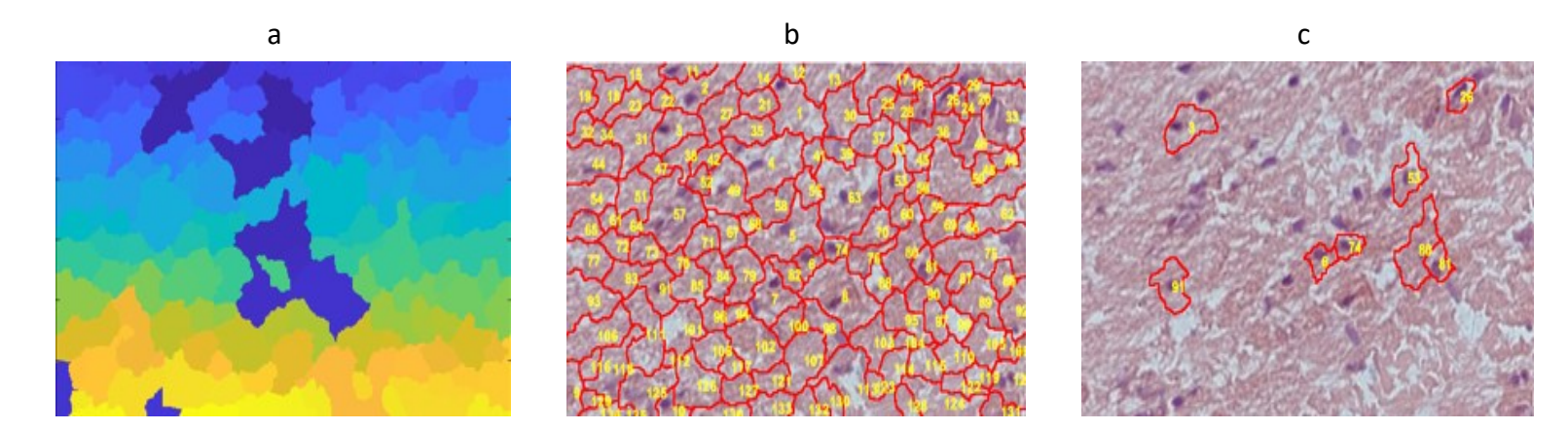


**Figure 13.a)** Watershed-segmented H&E-stained multimodal IMS mouse brain tissue section 1, **b)** cropped region of the same section, and **c)** isolated whole cells extracted from the cropped area.

Figure 13a represents the CSGO-segmented, cropped Hematoxylin and Eosin-stained multimodal IMS tissue section. Figure 13a shows the initial watershed segmentation output, where each color-coded region represents a potential cell-segmented region based on nuclear morphology. Figure 13b displays a boundary mask generated from the watershed output, overlaid onto the corresponding cropped H&E-stained image, highlighting the spatial alignment of segmented regions with histological features. Figure 13c presents the same overlaid image but with only fully segmented (whole) cells retained, excluding partial cells at the image borders, to ensure accuracy and reliability for subsequent single-cell molecular analysis.

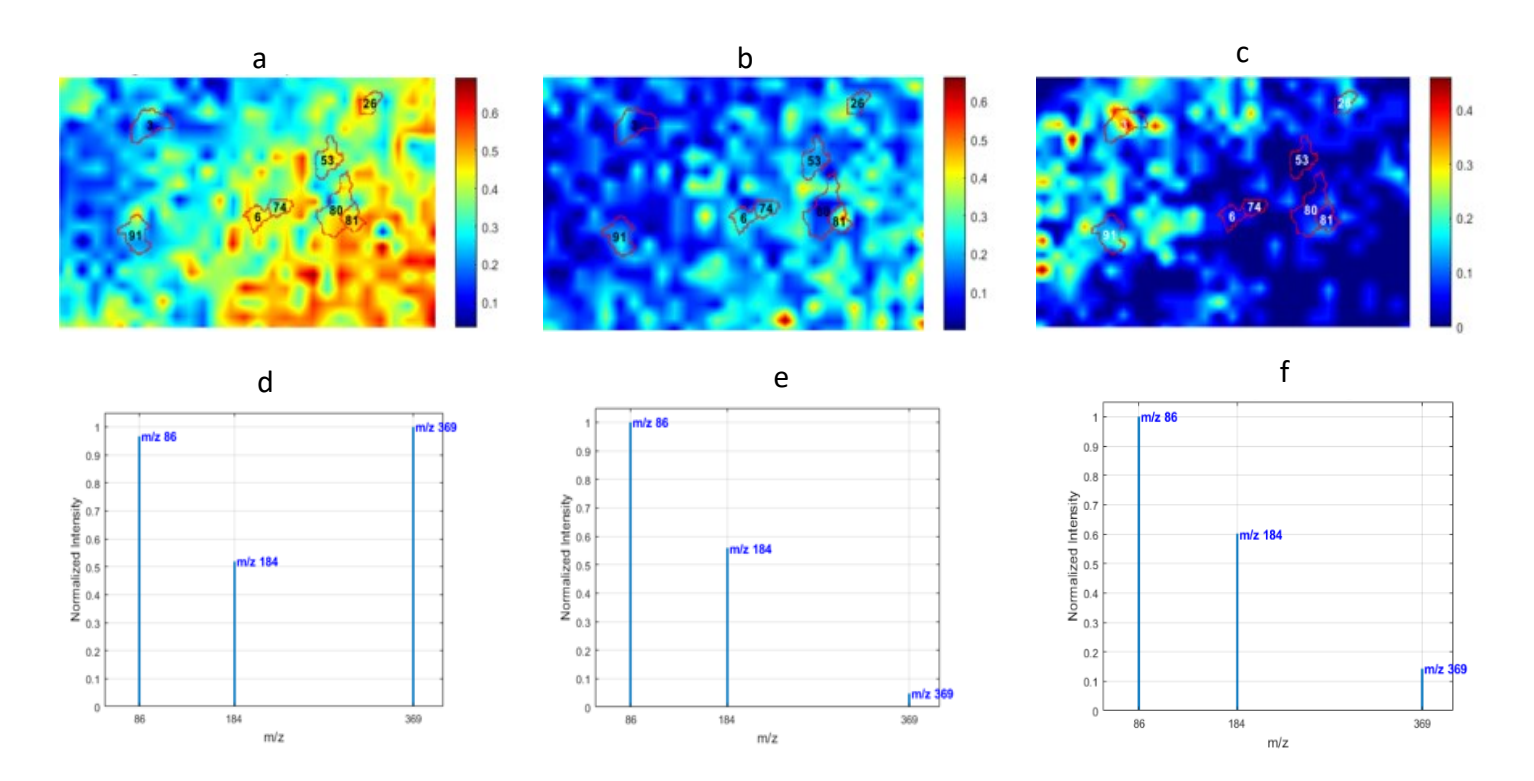


**Figure 14. a-c)** Overlay of isolated cell boundaries on the cropped, registered ToF-SIMS mouse brain ion images for m/z 86, 184, and 369, respectively; **d-f)** corresponding mass spectra for each cell.

**Figures 14a, 14b, and 14c** represent ToF-SIMS ion images showing the spatial distribution of three selected molecular species at m/z 86, m/z 184, and m/z 369, respectively. Each heatmap is color-coded to indicate normalized ion intensity, with warmer colors (red/yellow) representing higher intensity and cooler colors (blue) indicating lower intensity. Superimposed on each ion image are boundary masks outlining segmented single cells, labeled with unique region identifiers (e.g., 81, 74, 53), obtained from deep learning-based segmentation of the corresponding multimodal IMS H&E-stained image, and the ToF-SIMS images were subsequently registered to the multimodal IMS H&E coordinate space using laser-etched fiducial markers. **Figures 14d, 14e,** 

and 14f show individual mass spectra extracted from the highlighted single cells in each image above for regions 3, 74, and 81, respectively. These spectra display normalized intensity values for the selected m/z peaks (86, 184, and 369), showing their relative abundance within each cell. Differences in molecular composition can be observed between cells (highlighted by the segmented image). Figures 14e and 14f show the mass spectra for cells 74 and 81, respectively. Both cells exhibit prominent signals at m/z 86 and m/z 184, corresponding to phosphocholinerelated fragments, while the signal at m/z 369 (cholesterol) is comparatively low. This aligns with a gray matter molecular profile, where phospholipid-rich neuronal membranes and synaptic structures dominate. Support for this comes from studies by Berrueta et al., who demonstrated that the phosphocholine fragment at m/z 184 is strongly localized to gray matter regions in rat brain using ToF-SIMS, and Dowlatshahi Pour et al., who also reported robust phosphocholine signals in gray matter under both control and diet-induced conditions.[141] [142] Conversely, Figure 14d, showing cell 3, displays a strong signal at m/z 369, suggesting a white matter molecular phenotype characterized by high cholesterol content in myelin sheaths that insulate axons. This spatial distribution of cholesterol matches findings from studies using cluster ion beam ToF-SIMS, which show cholesterol fragments (m/z 369) enriched in myelinated white matter tracts.[143] Additional research has demonstrated that cholesterol detection can be further enhanced with gas cluster beam doped water, reinforcing its specific localization in white matter structures.[144] Note that several technical aspects need to be considered in this data, which can be improved with specific technical advances, e.g., (Increased ionization efficiency, sputtering yield), which could provide more robust and accurate biological information on single-cell IMS. In addition, segmenting single cells from tissue exposed to IMS vacuum conditions presents unique challenges. Vacuum-induced deformation can obscure cell boundaries, reducing segmentation accuracy. Therefore, machine

learning algorithms should be specifically trained on post-IMS tissue images to account for these morphological alterations and improve cell boundary detection under such conditions.

## **Chapter 4: Discussion and Future Direction**

### 4.1 Summary

This research aimed to develop protocols for integrating imaging mass spectrometry (IMS) techniques, such as Secondary Ion Mass Spectrometry (SIMS) and Matrix-assisted Laser Desorption/Ionization (MALDI), with hematoxylin and eosin-stained optical microscopy to enable spatially resolved, single-cell molecular analysis of mouse brain tissue. The study began by optimizing an optimal hematoxylin and eosin (H&E) staining protocol. This was followed by establishing a coregistration framework that aligned ion images from SIMS and MALDI with highresolution histological images. An initial analysis was conducted using consecutive tissue sections, where one section underwent multimodal IMS followed by H&E staining, and the adjacent section was stained directly with H&E. Coregistration between these two sections was performed using intrinsic tissue features, such as anatomical landmarks, to align nuclei between samples. While this approach yielded a general tissue-level alignment, further examination revealed a mismatch at the single-cell level, particularly in the positioning and morphology of nuclei. This was quantitatively confirmed by a Jaccard similarity index of 0.026, indicating minimal overlap between corresponding nuclear masks. This discrepancy was likely due to slight differences introduced during tissue sectioning, mounting, IMS experiment, or staining processes, which can lead to deformation or spatial displacement between adjacent sections. The observed misalignment underscored a critical limitation of using consecutive sections for single-cell resolution analyses, especially in applications involving molecular image overlays such as IMS. As a result, the study pivoted toward a same-tissue multimodal IMS strategy, wherein all imaging modalities (SIMS, MALDI, and H&E) were performed on the same tissue section. To enhance registration precision, a laser-etched fiducial marker system was employed on the glass slide before tissue mounting.

These fiducial markers served as stable, unchanging reference points across all imaging modalities. This refined approach enabled consistent alignment of cellular structures and laid the foundation for reliable single-cell molecular mapping across modalities. However, we were limited in our single-cell analysis by the spatial resolution of the TOF-MALDI instrument, which operated at 35 μm, exceeding the average diameter of a mouse brain cell (~10- 15 μm).[145] Consequently, MALDI data could not be reliably used for single-cell level localization. Therefore, we proceeded with ToF-SIMS for single-cell analysis, as it provided a higher spatial resolution (10 μm). Despite this advantage, ToF-SIMS analysis was constrained by the low abundance of secondary ions, due to the use of a liquid metal ion gun (LMIG) equipped only with Bi<sub>3</sub>+ ions. This configuration yielded suboptimal ion intensity, limiting sensitivity and the range of detectable molecular species in some regions.

This study employed a single-sample workflow, collecting three consecutive 10-µm mouse brain tissue sections initially to assess inter-section alignment at the single-cell level. Although the sections originated from the same tissue block, comparison of nuclear masks showed significant misalignment at the single-cell level, leading to a switch to a same-section multimodal strategy. While this approach (n = 1) is common in IMS method development due to the technical and resource demands of the experiments, reproducibility was maintained through standardized preparation protocols, consistent acquisition settings, and alignment with findings from previous studies. Future research should include technical and biological replicates to better validate and extend the proposed workflow.

Additionally, although we only extracted ion intensities for three m/z values (86, 184, and 369) to demonstrate proof-of-concept single-cell spectral analysis, this method can easily be expanded to include a wider range of m/z values, resulting in more comprehensive and information-rich spectra

for each cell. Nonetheless, by combining fiducial marker-based image registration, deep learning-based segmentation, and pixel-resolved SIMS intensity extraction, this study offers a reliable and reproducible workflow for linking histological features with molecular data at the single-cell level.

### 4.2 The Role of Integrated Tissue Analysis in Molecular Pathology

Molecular pathology is a rapidly expanding component of the discipline of pathology that uses molecular biology tools in addition to conventional morphologic, immunohistochemical, and chemical analyses of abnormalities in tissues and cells to understand the etiology and pathogenesis of tumors, establish their diagnosis, and contribute to prognostication and therapeutic decisions for cancer patient care.[146] In contrast, histopathology enables the study of diseased tissue using sectioning, staining, and multi-resolution microscopy.[147] It involves analyzing tissue samples to understand disease processes, diagnose conditions, and guide treatment decisions.[148] Traditional histopathology, while indispensable for diagnosing structural and cellular abnormalities, is largely focused on visual assessment of morphological features. The integration of high-resolution histological imaging with molecular imaging technologies, such as SIMS and MALDI, represents a transformative shift in how tissue samples are analyzed and interpreted in molecular pathology. This thesis contributes to the advancement of molecular pathology by demonstrating a workflow that spatially correlates histological structures with mass spectrometryderived molecular data at single-cell resolution using laser-etched fiducial markers for improved spatial alignment.

IMS provides distinct advantages over other imaging modalities, such as immunohistochemistry (IHC) and fluorescence microscopy, by offering label-free, untargeted tissue analysis - It emerged as a response to the demand for spatial information about biomolecules detected by conventional

mass spectrometry.[149] Techniques such as secondary ion mass spectrometry (SIMS) offer subcellular molecular imaging down to 10 nm[21], enhancing histological assessments.

IMS-based molecular pathology would provide significant applications across various fields. In pharmacological research, IMS enables the examination of the distribution of biologically active substances and their metabolites in the body, as IMS approaches avoid complex and extensive sample preparation, thereby preserving the distribution of substances in the samples.[150] Additionally, IMS has emerged as a transformative tool in cancer research, offering unprecedented capabilities for understanding, detecting, and treating cancer.[151] Ultimately, this technology enables researchers to identify and validate potential biomarkers while preserving their spatial context, providing advantages over traditional analytical methods.[152]

Although instrumental constraints limit certain aspects of our analysis, the overall methodology clearly illustrates the potential of combining histological imaging with mass spectrometry to generate spatially resolved molecular profiles at the single-cell level. Future improvements, such as higher-resolution instruments and multi-ion beam systems, will further broaden the applicability of this pipeline in both research and clinical pathology settings.

In conclusion, combining imaging mass spectrometry with optical microscopy of histologically stained mouse brain tissue facilitated by laser-etched fiducial markers for enhanced image coregistration marks a major progress in molecular pathology. This method not only deepens our understanding of tissue biology but also offers potential for more precise, cell-level diagnostics and personalized treatment options.

### 4.3 Possible Future Direction

This study demonstrated the feasibility and benefits of integrating IMS with histological analysis for molecular pathology applications. However, several pathways remain available to further improve or enhance the accuracy, reproducibility, and applicability of the methodologies examined in this research.

One critical aspect that requires improvement is the data processing workflow. In this study, data were processed using R, Python, and MATLAB; however, direct reading of the imzML file format into MATLAB proved challenging, necessitating additional conversion steps. Future research could focus on developing streamlined pipelines that enable the direct import of imzML files into MATLAB, thereby eliminating the need for intermediate conversions and simplifying processing complexity. One approach could be the development of dedicated MATLAB functions or toolboxes specifically designed to support the reading and processing of imzML files. Additionally, Researchers should explore the expansion of IMS methods through the combination of various multimodal imaging techniques. Our study examined Secondary Ion Mass Spectrometry (SIMS) and Matrix-Assisted Laser Desorption Ionization (MALDI). Yet, future research could gain from incorporating Desorption Electrospray Ionization (DESI), Infrared Matrix-Assisted Laser Desorption Electrospray Ionization (IR-MALDESI), spatial transcriptomics, and genomics techniques. Another important consideration is to optimize the workflow for detecting proteins using MALDI-TOF. In this study, dry matrix sublimation with 1,5-diaminonaphthalene was used, which favors small molecules like lipids but is less effective for protein ionization.[153] Future research could enhance protein detection by using protein-optimized matrices such as sinapinic acid or ferulic acid.[154] Finally, it is important to optimize the H&E staining protocol for tissue sections that have undergone multimodal IMS analysis, particularly to account for the structural

and chemical alterations induced by prior exposure to vacuum conditions. Improving the quality of the resulting optical microscopy images will directly enhance the performance of deep learning-based cell segmentation methods, enabling more accurate and reliable single-cell analysis.

Complementary methods enable researchers to achieve more detailed molecular profiles from tissue samples, leading to a better understanding of the spatial distribution of biomolecules. Additionally, the protocol developed in this study for multimodal IMS-histology integration could be applied to other histological stains and organ types in future research. Using this approach for different tissues, such as the liver, kidney, or lung, could promote broader applications in biomedical and clinical studies. This expansion could provide a more comprehensive understanding of disease pathology and biomarker distribution across diverse organ systems.

#### References

- [1] E. R. Amstalden van Hove, D. F. Smith, and R. M. A. Heeren, "A concise review of mass spectrometry imaging," *Journal of Chromatography A*, vol. 1217, no. 25, pp. 3946–3954, Jun. 2010, doi: 10.1016/j.chroma.2010.01.033.
- [2] C. Bich, D. Touboul, and A. Brunelle, "Cluster TOF-SIMS imaging as a tool for micrometric histology of lipids in tissue," *Mass Spectrometry Reviews*, vol. 33, no. 6, pp. 442–451, 2014, doi: 10.1002/mas.21399.
- [3] "Multimodal Imaging Mass Spectrometry: Next Generation Molecular Mapping in Biology and Medicine | Journal of the American Society for Mass Spectrometry." Accessed: Aug. 22, 2024. [Online]. Available: https://pubs.acs.org/doi/full/10.1021/jasms.0c00232
- [4] R. M. Caprioli, "Imaging Mass Spectrometry: A Perspective," *J Biomol Tech*, vol. 30, no. 1, pp. 7–11, Apr. 2019, doi: 10.7171/jbt.19-3001-002.
- [5] A. Bodzon-Kulakowska and P. Suder, "Imaging mass spectrometry: Instrumentation, applications, and combination with other visualization techniques," *Mass Spectrometry Reviews*, vol. 35, no. 1, pp. 147–169, 2016, doi: 10.1002/mas.21468.
- [6] "Molecular Imaging of Biological Samples: Localization of Peptides and Proteins Using MALDI-TOF MS | Analytical Chemistry." Accessed: Aug. 22, 2024. [Online]. Available: https://pubs.acs.org/doi/full/10.1021/ac970888i
- [7] A. Moerman *et al.*, "Lipid signature of advanced human carotid atherosclerosis assessed by mass spectrometry imaging," *Journal of Lipid Research*, vol. 62, p. jlr.RA120000974, Dec. 2020, doi: 10.1194/jlr.RA120000974.
- [8] A. P. Bowman *et al.*, "Evaluation of lipid coverage and high spatial resolution MALDI-imaging capabilities of oversampling combined with laser post-ionisation," *Anal Bioanal Chem*, vol. 412, no. 10, pp. 2277–2289, Apr. 2020, doi: 10.1007/s00216-019-02290-3.
- [9] J. A. Fincher *et al.*, "Mass Spectrometry Imaging of Lipids in Human Skin Disease Model Hidradenitis Suppurativa by Laser Desorption Ionization from Silicon Nanopost Arrays," *Sci Rep*, vol. 9, no. 1, p. 17508, Nov. 2019, doi: 10.1038/s41598-019-53938-0.
- [10] M. L. Spruill, M. Maletic-Savatic, H. Martin, F. Li, and X. Liu, "Spatial analysis of drug absorption, distribution, metabolism, and toxicology using mass spectrometry imaging," *Biochemical Pharmacology*, vol. 201, p. 115080, Jul. 2022, doi: 10.1016/j.bcp.2022.115080.
- [11] D. Bonnel *et al.*, "MALDI imaging facilitates new topical drug development process by determining quantitative skin distribution profiles," *Analytical and Bioanalytical Chemistry*, vol. 410, no. 11, pp. 2815–2828, Apr. 2018, doi: 10.1007/s00216-018-0964-3.
- [12] J. Griffiths, "Secondary Ion Mass Spectrometry," *Anal. Chem.*, vol. 80, no. 19, pp. 7194–7197, Oct. 2008, doi: 10.1021/ac801528u.
- [13] A. M. Belu, D. J. Graham, and D. G. Castner, "Time-of-flight secondary ion mass spectrometry: techniques and applications for the characterization of biomaterial surfaces," *Biomaterials*, vol. 24, no. 21, pp. 3635–3653, Sep. 2003, doi: 10.1016/S0142-9612(03)00159-5.
- [14] D. S. McPhail, "Applications of Secondary Ion Mass Spectrometry (SIMS) in Materials Science," *J Mater Sci*, vol. 41, no. 3, pp. 873–903, Feb. 2006, doi: 10.1007/s10853-006-6568-x.
- [15] "Imaging lipids with secondary ion mass spectrometry ScienceDirect." Accessed: Sep. 07, 2024. [Online]. Available:

- https://www.sciencedirect.com/science/article/pii/S1388198114000444?casa\_token=jNr2Y AYqZMkAAAAA:qxPigg4RzFxYtYNh4hGphQX\_zy0guq0taPh4QbX1\_Sg8BHZFccJkdh YRZsRrssDWmhzKHKSs1feg
- [16] J. Nuñez, R. Renslow, J. B. Cliff III, and C. R. Anderton, "NanoSIMS for biological applications: Current practices and analyses," *Biointerphases*, vol. 13, no. 3, p. 03B301, Sep. 2017, doi: 10.1116/1.4993628.
- [17] Z. Shen and S. Fearn, "Back-to-basics tutorial: Secondary ion mass spectrometry (SIMS) in ceramics," *J Electroceram*, Dec. 2024, doi: 10.1007/s10832-024-00375-9.
- [18] S. L. Luxembourg, T. H. Mize, L. A. McDonnell, and R. M. A. Heeren, "High-Spatial Resolution Mass Spectrometric Imaging of Peptide and Protein Distributions on a Surface," *Anal. Chem.*, vol. 76, no. 18, pp. 5339–5344, Sep. 2004, doi: 10.1021/ac049692q.
- [19] A. Römpp and B. Spengler, "Mass spectrometry imaging with high resolution in mass and space," *Histochemistry and Cell Biology*, vol. 139, no. 6, pp. 759–783, Jun. 2013, doi: 10.1007/s00418-013-1097-6.
- [20] "Introduction to mass spectrometry imaging data analysis | Aspect Analytics | Bring your spatial multi-omics data together." Accessed: Mar. 19, 2025. [Online]. Available: https://www.aspect-analytics.com/media-blog/introduction-to-mass-spectrometry-imaging-data-analysis
- [21] C. W. Mueller *et al.*, "Submicron scale imaging of soil organic matter dynamics using NanoSIMS From single particles to intact aggregates," *Organic Geochemistry*, vol. 42, no. 12, pp. 1476–1488, Jan. 2012, doi: 10.1016/j.orggeochem.2011.06.003.
- [22] X. Xu *et al.*, "Application of high-spatial-resolution secondary ion mass spectrometry for nanoscale chemical mapping of lithium in an Al-Li alloy," *Materials Characterization*, vol. 181, p. 111442, Nov. 2021, doi: 10.1016/j.matchar.2021.111442.
- [23] F. Jia, X. Zhao, and Y. Zhao, "Advancements in ToF-SIMS imaging for life sciences," *Frontiers in Chemistry*, vol. 11, Aug. 2023, doi: 10.3389/fchem.2023.1237408.
- [24] D. Touboul and A. Brunelle, "TOF-SIMS imaging of lipids on rat brain sections," *Methods Mol Biol*, vol. 1203, pp. 21–27, 2015, doi: 10.1007/978-1-4939-1357-2\_3.
- [25] M. D. Pour, L. Ren, E. Jennische, S. Lange, A. G. Ewing, and P. Malmberg, "Mass spectrometry imaging as a novel approach to measure hippocampal zinc," *Journal of Analytical Atomic Spectrometry*, vol. 34, no. 8, pp. 1581–1587, 2019, doi: 10.1039/C9JA00199A.
- [26] A. N. Lazar *et al.*, "Time-of-flight secondary ion mass spectrometry (TOF-SIMS) imaging reveals cholesterol overload in the cerebral cortex of Alzheimer disease patients," *Acta Neuropathol*, vol. 125, no. 1, pp. 133–144, Jan. 2013, doi: 10.1007/s00401-012-1041-1.
- [27] F. Hillenkamp and J. Peter-Katalinic, *MALDI MS: A Practical Guide to Instrumentation, Methods and Applications*. John Wiley & Sons, 2013.
- [28] I. Rzagalinski and D. A. Volmer, "Quantification of low molecular weight compounds by MALDI imaging mass spectrometry A tutorial review," *Biochimica et Biophysica Acta (BBA) Proteins and Proteomics*, vol. 1865, no. 7, pp. 726–739, Jul. 2017, doi: 10.1016/j.bbapap.2016.12.011.
- [29] H. Räder and W. Schrepp, "MALDI-TOF mass spectrometry in the analysis of synthetic polymers," *Acta Polymerica*, vol. 49, no. 6, pp. 272–293, 1998, doi: 10.1002/(SICI)1521-4044(199806)49:6<272::AID-APOL272>3.0.CO;2-1.

- [30] L. S. Ferguson, S. Creasey, R. Wolstenholme, M. R. Clench, and S. Francese, "Efficiency of the dry—wet method for the MALDI-MSI analysis of latent fingermarks," *Journal of Mass Spectrometry*, vol. 48, no. 6, pp. 677–684, 2013, doi: 10.1002/jms.3216.
- [31] K. Dreisewerd, "Recent methodological advances in MALDI mass spectrometry," *Anal Bioanal Chem*, vol. 406, no. 9, pp. 2261–2278, Apr. 2014, doi: 10.1007/s00216-014-7646-6.
- [32] R. B. Cole, *Electrospray and MALDI Mass Spectrometry: Fundamentals, Instrumentation, Practicalities, and Biological Applications.* John Wiley & Sons, 2011.
- [33] "MALDI-TOF Mass Spectrometry in Clinical Analysis and Research | ACS Measurement Science Au." Accessed: Sep. 08, 2024. [Online]. Available: https://pubs-acs-org.lib-ezproxy.concordia.ca/doi/full/10.1021/acsmeasuresciau.2c00019
- [34] "New Analysis Workflow for MALDI Imaging Mass Spectrometry: Application to the Discovery and Identification of Potential Markers of Childhood Absence Epilepsy | Journal of Proteome Research." Accessed: Sep. 09, 2024. [Online]. Available: https://pubs.acs.org/doi/full/10.1021/pr3006974?casa\_token=BBrq0UtJ5NkAAAAA%3AZ dm92ZuBeRnWEO7iDFLcV-3TKL6AgFKAMJIbudhjvXHEmMv SK2stFXFzuyJNKZ8jQWW1dOiiBfMNmuecg#
- [35] D. Rinaldi, A. Depaulis, and B. Martin, "JLE Epilepsies The BS/ENT and BR/ENT mouse lines: two genetic models of epilepsy-absence and resistance to epilepsy-absence", Accessed: Jul. 04, 2025. [Online]. Available: https://www.jle.com/fr/revues/epi/edocs/les\_lignees\_de\_souris\_bs\_orl\_et\_br\_orl\_deux\_modeles\_genetiques\_d\_epilepsie\_absences et de resistance a l epilepsie absences 120081/article.phtml?cle doc=0001D511
- [36] "Imaging of peptides in the rat brain using MALDI-FTICR mass spectrometry | Journal of the American Society for Mass Spectrometry." Accessed: Sep. 09, 2024. [Online]. Available: https://pubs.acs.org/doi/abs/10.1016/j.jasms.2006.09.017?casa\_token=ltnJ3gyGnhQAAAA A:XP50v3C3cPB9b6waXblVs82VrMmxNxcgX97nHQmlS0sspDDzO6DMDxvuWzJHupg M1H8oSgvLaEp02FA6jg
- [37] "MALDI imaging mass spectrometry: Spatial molecular analysis to enable a new age of discovery ScienceDirect." Accessed: Sep. 09, 2024. [Online]. Available: https://www-sciencedirect-com.lib-ezproxy.concordia.ca/science/article/pii/S1874391914001432?casa\_token=BwDH-1vPtPQAAAAA:EoHQ4AgaVqzkTc\_XhOtPd5K0DJjpTR2LQKaAIJg87F8JJ3S8nxqSEnogg-WvmI4hIjzCEfsOTmAb
- [38] "CS22-1c.pdf." Accessed: Sep. 09, 2024. [Online]. Available: http://currentseparations.com/issues/22-1/CS22-1c.pdf
- [39] B. Sampath Kumar, "Desorption electrospray ionization mass spectrometry imaging (DESI-MSI) in disease diagnosis: an overview," *Analytical Methods*, vol. 15, no. 31, pp. 3768–3784, 2023, doi: 10.1039/D3AY00867C.
- [40] A. Ajith, Y. Sthanikam, and S. Banerjee, "Chemical analysis of the human brain by imaging mass spectrometry", doi: 10.1039/D1AN01109J.
- [41] N. M. Morato and R. G. Cooks, "Desorption Electrospray Ionization Mass Spectrometry: 20 Years," *Acc. Chem. Res.*, vol. 56, no. 18, pp. 2526–2536, Sep. 2023, doi: 10.1021/acs.accounts.3c00382.

- [42] C. L. Feider, A. Krieger, R. J. DeHoog, and L. S. Eberlin, "Ambient Ionization Mass Spectrometry: Recent Developments and Applications," *Anal. Chem.*, vol. 91, no. 7, pp. 4266–4290, Apr. 2019, doi: 10.1021/acs.analchem.9b00807.
- [43] L. S. Eberlin, C. R. Ferreira, A. L. Dill, D. R. Ifa, and R. G. Cooks, "Desorption electrospray ionization mass spectrometry for lipid characterization and biological tissue imaging," *Biochimica et Biophysica Acta (BBA) Molecular and Cell Biology of Lipids*, vol. 1811, no. 11, pp. 946–960, Nov. 2011, doi: 10.1016/j.bbalip.2011.05.006.
- [44] "Ambient mass spectrometry using desorption electrospray ionization (DESI): instrumentation, mechanisms and applications in forensics, chemistry, and biology Takáts 2005 Journal of Mass Spectrometry Wiley Online Library." Accessed: Sep. 10, 2024. [Online]. Available: https://analyticalsciencejournals-onlinelibrary-wiley-com.lib-ezproxy.concordia.ca/doi/full/10.1002/jms.922?casa\_token=w3JyazDO4ygAAAAA%3Auq qNFiYa5KtD3hhGyBy3MgAA758JYUX4unxWEMvQc\_\_GhaU\_9FHcmnsHf7MXWvpjn 7GBFN mkmOZok0m7g
- [45] "Review and perspectives on the applications of mass spectrometry imaging under ambient conditions Perez 2019 Rapid Communications in Mass Spectrometry Wiley Online Library." Accessed: Sep. 10, 2024. [Online]. Available: https://analyticalsciencejournals-onlinelibrary-wiley-com.lib-ezproxy.concordia.ca/doi/full/10.1002/rcm.8145?casa\_token=hZoEvK6z60YAAAAA%3A vnfznXVeaaF6-8kJwl9LI9V8khDDG4BT81Sx8eoDljoKIGdHW3mCXSPo85dLZoYkHeX7DpzKWjbPW Ykupw
- [46] D. I. Campbell, C. R. Ferreira, L. S. Eberlin, and R. G. Cooks, "Improved spatial resolution in the imaging of biological tissue using desorption electrospray ionization," *Anal Bioanal Chem*, vol. 404, no. 2, pp. 389–398, Aug. 2012, doi: 10.1007/s00216-012-6173-6.
- [47] H. Ageta, S. Asai, Y. Sugiura, N. Goto-Inoue, N. Zaima, and M. Setou, "Layer-specific sulfatide localization in rat hippocampus middle molecular layer is revealed by nanoparticle-assisted laser desorption/ionization imaging mass spectrometry," *Med Mol Morphol*, vol. 42, no. 1, pp. 16–23, Mar. 2009, doi: 10.1007/s00795-008-0427-6.
- [48] S. Sengaloundeth *et al.*, "A stratified random survey of the proportion of poor quality oral artesunate sold at medicine outlets in the Lao PDR implications for therapeutic failure and drug resistance," *Malar J*, vol. 8, p. 172, Jul. 2009, doi: 10.1186/1475-2875-8-172.
- [49] C. Zhao, L. Guo, J. Dong, and Z. Cai, "Mass spectrometry imaging-based multi-modal technique: Next-generation of biochemical analysis strategy," *The Innovation*, vol. 2, no. 4, p. 100151, Nov. 2021, doi: 10.1016/j.xinn.2021.100151.
- [50] B. Zitová and J. Flusser, "Image registration methods: a survey," *Image and Vision Computing*, vol. 21, no. 11, pp. 977–1000, Oct. 2003, doi: 10.1016/S0262-8856(03)00137-9.
- [51] "Frontiers | MALDI-MSI Towards Multimodal Imaging: Challenges and Perspectives." Accessed: Sep. 11, 2024. [Online]. Available: https://www.frontiersin.org/journals/chemistry/articles/10.3389/fchem.2022.904688/full#B 84
- [52] S. Chughtai *et al.*, "A multimodal mass spectrometry imaging approach for the study of musculoskeletal tissues," *International Journal of Mass Spectrometry*, vol. 325–327, pp. 150–160, Jul. 2012, doi: 10.1016/j.ijms.2012.07.008.

- [53] I. Vermeulen, E. M. Isin, P. Barton, B. Cillero-Pastor, and R. M. A. Heeren, "Multimodal molecular imaging in drug discovery and development," *Drug Discovery Today*, vol. 27, no. 8, pp. 2086–2099, Aug. 2022, doi: 10.1016/j.drudis.2022.04.009.
- [54] L. E. M. Tideman *et al.*, "Automated biomarker candidate discovery in imaging mass spectrometry data through spatially localized Shapley additive explanations," *Analytica Chimica Acta*, vol. 1177, p. 338522, Sep. 2021, doi: 10.1016/j.aca.2021.338522.
- [55] "Histology Guide virtual microscopy laboratory." Accessed: Mar. 20, 2025. [Online]. Available: https://histologyguide.com/
- [56] "Fulltext | Past, present and future: overview on histology and histopathology | Journal of Histology & Histopathology." Accessed: Sep. 11, 2024. [Online]. Available: https://www.hoajonline.com/histology/2055-091X/1/5
- [57] I. Hussein, M. Raad, R. Safa, R. Jurjus, and A. Jurjus, "Once Upon a Microscopic Slide: The Story of Histology," *Journal of Cytology & Histology*, vol. 6, Jan. 2015, doi: 10.4172/2157-7099.1000377.
- [58] "Virtual Staining of Nonfixed Tissue Histology ScienceDirect." Accessed: Sep. 12, 2024. [Online]. Available: https://www-sciencedirect-com.lib-ezproxy.concordia.ca/science/article/pii/S0893395224000243
- [59] H. Ganjali and M. Ganjali, "Fixation in tissue processing," 2013.
- [60] R. Chandraker, V. C. Rathod, N. K. Chandraker, S. Pundir, S. Dixit, and V. Desai, "Comparison Between Xylene And Coconut Oil In Tissue Processing," *Modern Medical Laboratory Journal*, vol. 2, no. 1, pp. 96–99, Jan. 2019, doi: 10.30699/mmlj17.1.3.96.
- [61] "The Intersection of Epidemiology and Pathology | SpringerLink." Accessed: Sep. 12, 2024. [Online]. Available: https://link.springer.com/chapter/10.1007/978-3-319-35153-7\_1
- [62] J. S. Lowe, P. G. Anderson, and S. I. Anderson, *Stevens & Lowe's Human Histology E-Book: Stevens & Lowe's Human Histology E-Book.* Elsevier Health Sciences, 2023.
- [63] N. Pillar and A. Ozcan, "Virtual tissue staining in pathology using machine learning," *Expert Review of Molecular Diagnostics*, vol. 22, no. 11, pp. 987–989, Nov. 2022, doi: 10.1080/14737159.2022.2153040.
- [64] R. D. Cardiff, C. H. Miller, and R. J. Munn, "Manual Hematoxylin and Eosin Staining of Mouse Tissue Sections," *Cold Spring Harb Protoc*, vol. 2014, no. 6, p. pdb.prot073411, Jun. 2014, doi: 10.1101/pdb.prot073411.
- [65] A. T. Feldman and D. Wolfe, "Tissue Processing and Hematoxylin and Eosin Staining," in *Histopathology: Methods and Protocols*, C. E. Day, Ed., New York, NY: Springer, 2014, pp. 31–43. doi: 10.1007/978-1-4939-1050-2\_3.
- [66] T. S. Gurina and L. Simms, "Histology, Staining," in *StatPearls*, Treasure Island (FL): StatPearls Publishing, 2024. Accessed: Sep. 16, 2024. [Online]. Available: http://www.ncbi.nlm.nih.gov/books/NBK557663/
- [67] "Tissue Processing Overview: Steps & Techniques for Histopathology." Accessed: Sep. 16, 2024. [Online]. Available: https://www.leicabiosystems.com/knowledge-pathway/an-introduction-to-specimen-processing/
- [68] "Pathology Research Core Tissue Sectioning," Mayo Clinic. Accessed: Sep. 16, 2024. [Online]. Available: https://www.mayo.edu/research/core-resources/pathology-research-core/services/tissue-sectioning
- [69] "Paraffin & Frozen Sectioning | Histology Research Core." Accessed: Sep. 16, 2024. [Online]. Available: https://histologyresearchcorefacility.web.unc.edu/paraffin-frozen-sectioning/

- [70] mmldigi, "Microtome Sectioning of Tissue- RWD Science," RWD Life Science. Accessed: Sep. 16, 2024. [Online]. Available: https://www.rwdstco.com/microtome-sectioning-of-tissue/
- [71] A. H. Fischer, K. A. Jacobson, J. Rose, and R. Zeller, "Paraffin Embedding Tissue Samples for Sectioning," *Cold Spring Harb Protoc*, vol. 2008, no. 5, p. pdb.prot4989, May 2008, doi: 10.1101/pdb.prot4989.
- [72] P. Dey, "Frozen Section: Principle and Procedure," in *Basic and Advanced Laboratory Techniques in Histopathology and Cytology*, P. Dey, Ed., Singapore: Springer, 2018, pp. 51–55. doi: 10.1007/978-981-10-8252-8 6.
- [73] N. Diagnostics, "Sectioning," National Diagnostics. Accessed: Sep. 16, 2024. [Online]. Available: https://www.nationaldiagnostics.com/2011/09/26/sectioning/
- [74] S. Renshaw, "Chapter 4.2 Immunohistochemistry and Immunocytochemistry," in *The Immunoassay Handbook (Fourth Edition)*, D. Wild, Ed., Oxford: Elsevier, 2013, pp. 357–377. doi: 10.1016/B978-0-08-097037-0.00024-5.
- [75] "Frozen Section an overview | ScienceDirect Topics." Accessed: Sep. 16, 2024. [Online]. Available: https://www-sciencedirect-com.lib-ezproxy.concordia.ca/topics/biochemistry-genetics-and-molecular-biology/frozen-section
- [76] R. Lott et al., "Practical Guide to Specimen Handling in Surgical Pathology," 2023.
- [77] "Frozen section overview." Accessed: Sep. 19, 2024. [Online]. Available: https://www.pathologyoutlines.com/topic/cytopathologyfrozen.html
- [78] "Histological techniques 5. Staining. General staining. Atlas of plant and animal histology." Accessed: Sep. 19, 2024. [Online]. Available: https://mmegias.webs.uvigo.es/02-english/6-tecnicas/5-general.php
- [79] Y. Zhang, K. de Haan, Y. Rivenson, J. Li, A. Delis, and A. Ozcan, "Digital synthesis of histological stains using micro-structured and multiplexed virtual staining of label-free tissue," *Light Sci Appl*, vol. 9, no. 1, p. 78, May 2020, doi: 10.1038/s41377-020-0315-y.
- [80] "Histological staining," Research and innovation. Accessed: Sep. 19, 2024. [Online]. Available: https://www.uottawa.ca/research-innovation/histology/services/histological-staining
- [81] "Routine & Special Staining Creative Bioarray." Accessed: Sep. 19, 2024. [Online]. Available: https://www.histobiolab.com/routine-special-staining.html
- [82] "Tissue Staining: Definition, Type & Structure | StudySmarter," StudySmarter UK. Accessed: Sep. 19, 2024. [Online]. Available: https://www.studysmarter.co.uk/explanations/biology/biological-structures/tissue-staining/
- [83] K. Larson, H. H. Ho, P. L. Anumolu, and T. M. Chen, "Hematoxylin and Eosin Tissue Stain in Mohs Micrographic Surgery: A Review," *Dermatologic Surgery*, vol. 37, no. 8, pp. 1089–1099, 2011, doi: 10.1111/j.1524-4725.2011.02051.x.
- [84] "Special Stains Miller School of Medicine." Accessed: Sep. 20, 2024. [Online]. Available: https://med.miami.edu/departments/comparative-pathology/divisions/pathology-research-resources/histology-research-laboratory/special-stains
- [85] J. Rosai, Rosai and Ackerman's Surgical Pathology E-Book. Elsevier Health Sciences, 2011.
- [86] "Application of Immunohistochemical Staining to Detect Antigen Destruction as a Measure of Tissue Damage Abdullah Onul, Michael D. Colvard, William A. Paradise, Kim M. Elseth, Benjamin J. Vesper, Eftychia Gouvas, Zane Deliu, Kelly D. Garcia, William J.

- Pestle, James A. Radosevich, 2012." Accessed: Sep. 20, 2024. [Online]. Available: https://journals.sagepub.com/doi/full/10.1369/0022155412452146
- [87] S. Ravikumar, R. Surekha, and R. Thavarajah, "Mounting media: An overview," *Journal of Dr. YSR University of Health Sciences*, vol. 3, no. Suppl 1, p. S1, Mar. 2014, doi: 10.4103/2277-8632.128479.
- [88] P. Brown, "A review of Techniques used in the preparation, curation and conservation of Microsciope slides at the Natural History Museum, London.," *The Biology Curator*, vol. 10, pp. 1–33, Jan. 1997.
- [89] "Non-aqueous mounting media Biotrend." Accessed: Dec. 17, 2024. [Online]. Available: https://www.biotrend.com/kauf/cat-non-aqueous-mounting-media-4122.html
- [90] P. J. Todd, T. G. Schaaff, P. Chaurand, and R. M. Caprioli, "Organic ion imaging of biological tissue with secondary ion mass spectrometry and matrix-assisted laser desorption/ionization," *Journal of Mass Spectrometry*, vol. 36, no. 4, pp. 355–369, 2001, doi: 10.1002/jms.153.
- [91] "Molecular Imaging of Biological Samples: Localization of Peptides and Proteins Using MALDI-TOF MS | Analytical Chemistry." Accessed: Oct. 01, 2024. [Online]. Available: https://pubs-acs-org.lib-ezproxy.concordia.ca/doi/10.1021/ac970888i
- [92] P. J. Todd, J. M. McMahon, R. T. Short, and C. A. McCandlish, "Organic SIMS of biologic tissue," *Anal Chem*, vol. 69, no. 17, pp. 529A-535A, Sep. 1997, doi: 10.1021/ac971763g.
- [93] I. Fournier, R. Day, and M. Salzet, "Direct Analyses of neuropeptides by in situ MALDI-TOF mass spectrometry in the rat brain," *Neuroendocrinology Letters*, vol. 1, no. 24, pp. 9–14, 2003.
- [94] K. Yanagisawa *et al.*, "Proteomic patterns of tumour subsets in non-small-cell lung cancer," *The Lancet*, vol. 362, no. 9382, pp. 433–439, Aug. 2003, doi: 10.1016/S0140-6736(03)14068-8.
- [95] I. Kaya, E. Jennische, S. Lange, and P. Malmberg, "Multimodal chemical imaging of a single brain tissue section using ToF-SIMS, MALDI-ToF and immuno/histochemical staining," *Analyst*, vol. 146, no. 4, pp. 1169–1177, 2021, doi: 10.1039/D0AN02172E.
- [96] "Integrating Histology and Imaging Mass Spectrometry | Analytical Chemistry." Accessed: Oct. 01, 2024. [Online]. Available: https://pubs-acs-org.lib-ezproxy.concordia.ca/doi/full/10.1021/ac0351264
- [97] "Direct analysis of laser capture microdissected cells by MALDI mass spectrometry | Journal of the American Society for Mass Spectrometry." Accessed: Oct. 01, 2024. [Online]. Available: https://pubs.acs.org/doi/abs/10.1016/S1044-0305(02)00644-X
- [98] K. Schwamborn, R. C. Krieg, M. Reska, G. Jakse, R. Knuechel, and A. Wellmann, "Identifying prostate carcinoma by MALDI-Imaging," *International Journal of Molecular Medicine*, vol. 20, no. 2, pp. 155–159, Aug. 2007, doi: 10.3892/ijmm.20.2.155.
- [99] S. Vianello, "Compatibility between TOF-SIMS lipid imaging and histological staining on a rat brain section," *Surface and Interface Analysis*, Jan. 2012, Accessed: Oct. 02, 2024. [Online]. Available: https://www.academia.edu/79555721/Compatibility\_between\_TOF\_SIMS\_lipid\_imaging\_a nd histological staining on a rat brain section
- [100]T. Alexandrov, "MALDI imaging mass spectrometry: statistical data analysis and current computational challenges," *BMC Bioinformatics*, vol. 13, no. 16, p. S11, Nov. 2012, doi: 10.1186/1471-2105-13-S16-S11.

- [101] T. Schramm *et al.*, "imzML A common data format for the flexible exchange and processing of mass spectrometry imaging data," *Journal of Proteomics*, vol. 75, no. 16, pp. 5106–5110, Aug. 2012, doi: 10.1016/j.jprot.2012.07.026.
- [102] A. Guo *et al.*, "SOmicsFusion: Multimodal coregistration and fusion between spatial metabolomics and biomedical imaging," *Artificial Intelligence Chemistry*, vol. 2, no. 1, p. 100058, Jun. 2024, doi: 10.1016/j.aichem.2024.100058.
- [103] L. Qu *et al.*, "Cross-modal coherent registration of whole mouse brains," *Nat Methods*, vol. 19, no. 1, pp. 111–118, Jan. 2022, doi: 10.1038/s41592-021-01334-w.
- [104] S. Yoon and T. G. Lee, "Biological tissue sample preparation for time-of-flight secondary ion mass spectrometry (ToF–SIMS) imaging," *Nano Convergence*, vol. 5, no. 1, p. 24, Sep. 2018, doi: 10.1186/s40580-018-0157-y.
- [105] "Direct profiling and imaging of plant metabolites in intact tissues by using colloidal graphite-assisted laser desorption ionization mass spectrometry Cha 2008 The Plant Journal Wiley Online Library." Accessed: Nov. 06, 2024. [Online]. Available: https://onlinelibrary-wiley-com.lib-ezproxy.concordia.ca/doi/full/10.1111/j.1365-313X.2008.03507.x
- [106] B. Balluff, R. M. A. Heeren, and A. M. Race, "An overview of image registration for aligning mass spectrometry imaging with clinically relevant imaging modalities," *Journal of Mass Spectrometry and Advances in the Clinical Lab*, vol. 23, pp. 26–38, Jan. 2022, doi: 10.1016/j.jmsacl.2021.12.006.
- [107] M. K. Passarelli and N. Winograd, "Lipid imaging with time-of-flight secondary ion mass spectrometry (ToF-SIMS)," *Biochimica et Biophysica Acta (BBA) Molecular and Cell Biology of Lipids*, vol. 1811, no. 11, pp. 976–990, Nov. 2011, doi: 10.1016/j.bbalip.2011.05.007.
- [108] E. R. Amstalden van Hove, D. F. Smith, and R. M. A. Heeren, "A concise review of mass spectrometry imaging," *Journal of Chromatography A*, vol. 1217, no. 25, pp. 3946–3954, Jun. 2010, doi: 10.1016/j.chroma.2010.01.033.
- [109] R. N. Alolga, S.-L. Wang, L.-W. Qi, H. Zang, and F.-Q. Huang, "MALDI mass spectrometry imaging in targeted drug discovery and development: The pros, the cons, and prospects in global omics techniques," *TrAC Trends in Analytical Chemistry*, vol. 178, p. 117860, Sep. 2024, doi: 10.1016/j.trac.2024.117860.
- [110] J. L. Norris and R. M. Caprioli, "Analysis of Tissue Specimens by Matrix-Assisted Laser Desorption/Ionization Imaging Mass Spectrometry in Biological and Clinical Research," *Chem. Rev.*, vol. 113, no. 4, pp. 2309–2342, Apr. 2013, doi: 10.1021/cr3004295.
- [111] A. Thomas, J. L. Charbonneau, E. Fournaise, and P. Chaurand, "Sublimation of New Matrix Candidates for High Spatial Resolution Imaging Mass Spectrometry of Lipids: Enhanced Information in Both Positive and Negative Polarities after 1,5-Diaminonapthalene Deposition," *Anal. Chem.*, vol. 84, no. 4, pp. 2048–2054, Feb. 2012, doi: 10.1021/ac2033547.
- [112] B. Bai, X. Yang, Y. Li, Y. Zhang, N. Pillar, and A. Ozcan, "Deep learning-enabled virtual histological staining of biological samples," *Light Sci Appl*, vol. 12, no. 1, p. 57, Mar. 2023, doi: 10.1038/s41377-023-01104-7.
- [113] K. S. Suvarna, C. Layton, and J. D. Bancroft, *Bancroft's Theory and Practice of Histological Techniques E-Book*. Elsevier Health Sciences, 2012.

- [114] A. H. Fischer, K. A. Jacobson, J. Rose, and R. Zeller, "Hematoxylin and Eosin Staining of Tissue and Cell Sections," *Cold Spring Harb Protoc*, vol. 2008, no. 5, p. pdb.prot4986, May 2008, doi: 10.1101/pdb.prot4986.
- [115] "An Intro to Routine and Special Staining in Histopathology." Accessed: Dec. 16, 2024. [Online]. Available: https://www.leicabiosystems.com/en-ca/knowledge-pathway/an-introduction-to-routine-and-special-staining/
- [116] A. M. Race, "Investigation and interpretation of large mass spectrometry imaging datasets".
- [117] E. A. Jones, S.-O. Deininger, P. C. W. Hogendoorn, A. M. Deelder, and L. A. McDonnell, "Imaging mass spectrometry statistical analysis," *Journal of Proteomics*, vol. 75, no. 16, pp. 4962–4989, Aug. 2012, doi: 10.1016/j.jprot.2012.06.014.
- [118] A. M. Race, R. T. Steven, A. D. Palmer, I. B. Styles, and J. Bunch, "Memory Efficient Principal Component Analysis for the Dimensionality Reduction of Large Mass Spectrometry Imaging Data Sets," *Anal. Chem.*, vol. 85, no. 6, pp. 3071–3078, Mar. 2013, doi: 10.1021/ac302528v.
- [119] A. Römpp *et al.*, "imzML: Imaging Mass Spectrometry Markup Language: A common data format for mass spectrometry imaging," *Methods Mol Biol*, vol. 696, pp. 205–224, 2011, doi: 10.1007/978-1-60761-987-1 12.
- [120] R. S. Bhamber, A. Jankevics, E. W. Deutsch, A. R. Jones, and A. W. Dowsey, "mzMLb: A Future-Proof Raw Mass Spectrometry Data Format Based on Standards-Compliant mzML and Optimized for Speed and Storage Requirements," *J. Proteome Res.*, vol. 20, no. 1, pp. 172–183, Jan. 2021, doi: 10.1021/acs.jproteome.0c00192.
- [121] "readBIF: ToF-SIMS BIF/BIF6 file import in tofsims: Import, process and analysis of Time-of-Flight Secondary Ion Mass Spectrometry (ToF-SIMS) imaging data." Accessed: Feb. 26, 2025. [Online]. Available: https://rdrr.io/bioc/tofsims/man/readBIF.html
- [122] M. Gardener, *Beginning R: The Statistical Programming Language*. John Wiley & Sons, 2012.
- [123] "Cardinal: an R package for statistical analysis of mass spectrometry-based imaging experiments PMC." Accessed: Feb. 27, 2025. [Online]. Available: https://pmc.ncbi.nlm.nih.gov/articles/PMC4495298/
- [124] "MATLAB." Accessed: Mar. 02, 2025. [Online]. Available: https://www.mathworks.com/products/matlab.html
- [125] "All You Need to Know About MATLAB (Matrix Laboratory)," Spiceworks Inc. Accessed: Mar. 02, 2025. [Online]. Available: https://www.spiceworks.com/tech/devops/articles/what-is-matlab/
- [126] N. Klingler, "Image Registration and Its Applications," viso.ai. Accessed: Mar. 04, 2025. [Online]. Available: https://viso.ai/computer-vision/image-registration/
- [127] M. Chen, N. J. Tustison, R. Jena, and J. C. Gee, "Image Registration: Fundamentals and Recent Advances Based on Deep Learning," in *Machine Learning for Brain Disorders*, O. Colliot, Ed., New York, NY: Humana, 2023. Accessed: Mar. 04, 2025. [Online]. Available: http://www.ncbi.nlm.nih.gov/books/NBK597490/
- [128] "academic-press-handbook-medical-imaging-processing-analysis.pdf." Accessed: Mar. 05, 2025. [Online]. Available: https://biblioseb.wordpress.com/wp-content/uploads/2018/03/academic-press-handbook-medical-imaging-processing-analysis.pdf

- [129] "document.pdf." Accessed: Mar. 05, 2025. [Online]. Available: https://citeseerx.ist.psu.edu/document?repid=rep1&type=pdf&doi=ca2afc1a252301837e21 8f739da1a9836ebf5fa7#page=17
- [130] "How to Calculate Jaccard Similarity in Python," GeeksforGeeks. Accessed: Mar. 06, 2025. [Online]. Available: https://www.geeksforgeeks.org/how-to-calculate-jaccard-similarity-in-python/
- [131] L. da F. Costa, "Further Generalizations of the Jaccard Index," Nov. 18, 2021, *arXiv*: arXiv:2110.09619. doi: 10.48550/arXiv.2110.09619.
- [132] H. Chen and R. F. Murphy, "Evaluation of cell segmentation methods without reference segmentations," *MBoC*, vol. 34, no. 6, p. ar50, May 2023, doi: 10.1091/mbc.E22-08-0364.
- [133] "Understanding Cell Segmentation: A Key Tool in Spatial Imagi...," Strand Life Sciences. Accessed: Mar. 08, 2025. [Online]. Available: https://us.strandls.com/blog/understanding-cell-segmentation-a-key-tool-in-spatial-imaging
- [134] B. Kochetov *et al.*, "UNSEG: unsupervised segmentation of cells and their nuclei in complex tissue samples," *Commun Biol*, vol. 7, no. 1, p. 1062, Aug. 2024, doi: 10.1038/s42003-024-06714-4.
- [135] "[No title found]," IJCSMC.
- [136] C. Kaushal, S. Bhat, D. Koundal, and A. Singla, "Recent Trends in Computer Assisted Diagnosis (CAD) System for Breast Cancer Diagnosis Using Histopathological Images," *IRBM*, vol. 40, no. 4, pp. 211–227, Aug. 2019, doi: 10.1016/j.irbm.2019.06.001.
- [137] M. S. Durkee, R. Abraham, M. R. Clark, and M. L. Giger, "Artificial Intelligence and Cellular Segmentation in Tissue Microscopy Images," *Am J Pathol*, vol. 191, no. 10, pp. 1693–1701, Oct. 2021, doi: 10.1016/j.ajpath.2021.05.022.
- [138] T. Wen *et al.*, "Review of research on the instance segmentation of cell images," *Computer Methods and Programs in Biomedicine*, vol. 227, p. 107211, Dec. 2022, doi: 10.1016/j.cmpb.2022.107211.
- [139] S. Miyaki, S. Nishimoto, Y. Tokuoka, T. G. Yamada, T. Morikura, and A. Funahashi, "Cell segmentation without annotation by unsupervised domain adaptation based on cooperative self-learning," Jul. 09, 2024, *bioRxiv*. doi: 10.1101/2024.07.05.602197.
- [140] Z. Gu *et al.*, "Cell Segmentation With Globally Optimized Boundaries (CSGO): A Deep Learning Pipeline for Whole-Cell Segmentation in Hematoxylin-and-Eosin-Stained Tissues," *Lab Invest*, vol. 105, no. 2, p. 102184, Feb. 2025, doi: 10.1016/j.labinv.2024.102184.
- [141] I. Berrueta Razo, S. Sheraz (née Rabbani), A. Henderson, N. P. Lockyer, and J. C. Vickerman, "Mass spectrometric imaging of brain tissue by time-of-flight secondary ion mass spectrometry How do polyatomic primary beams C60+, Ar2000+, water-doped Ar2000+ and (H2O)6000+ compare?," *Rapid Communications in Mass Spectrometry*, vol. 29, no. 20, pp. 1851–1862, 2015, doi: 10.1002/rcm.7285.
- [142] M. Dowlatshahi Pour, E. Jennische, S. Lange, A. G. Ewing, and P. Malmberg, "Foodinduced changes of lipids in rat neuronal tissue visualized by ToF-SIMS imaging," *Sci Rep*, vol. 6, no. 1, p. 32797, Sep. 2016, doi: 10.1038/srep32797.
- [143] K. Börner, H. Nygren, B. Hagenhoff, P. Malmberg, E. Tallarek, and J.-E. Månsson, "Distribution of cholesterol and galactosylceramide in rat cerebellar white matter," *Biochimica et Biophysica Acta (BBA) Molecular and Cell Biology of Lipids*, vol. 1761, no. 3, pp. 335–344, Mar. 2006, doi: 10.1016/j.bbalip.2006.02.021.

- [144] K. Dimovska Nilsson, A. Karagianni, I. Kaya, M. Henricsson, and J. S. Fletcher, "(CO2)n+, (H2O)n+, and (H2O)n+ (CO2) gas cluster ion beam secondary ion mass spectrometry: analysis of lipid extracts, cells, and Alzheimer's model mouse brain tissue," *Anal Bioanal Chem*, vol. 413, no. 16, pp. 4181–4194, Jul. 2021, doi: 10.1007/s00216-021-03372-x.
- [145] B. Krause, "Answer to 'What is the size of different mouse brain cells?," Biology Stack Exchange. Accessed: Mar. 19, 2025. [Online]. Available: https://biology.stackexchange.com/a/107103
- [146] S. R. Hamilton, "Molecular pathology," *Molecular Oncology*, vol. 6, no. 2, pp. 177–181, Apr. 2012, doi: 10.1016/j.molonc.2012.02.007.
- [147] T. R. C. of Pathologists, "Histopathology." Accessed: Jun. 30, 2025. [Online]. Available: https://www.rcpath.org/discover-pathology/news/fact-sheets/histopathology.html
- [148] "Histopathology," *Wikipedia*. Mar. 04, 2025. Accessed: Mar. 15, 2025. [Online]. Available: https://en.wikipedia.org/w/index.php?title=Histopathology&oldid=1278754141
- [149] K. Chughtai and R. M. A. Heeren, "Mass Spectrometric Imaging for Biomedical Tissue Analysis," *Chem. Rev.*, vol. 110, no. 5, pp. 3237–3277, May 2010, doi: 10.1021/cr100012c.
- [150] A. Bodzon-Kulakowska and P. Suder, "Imaging mass spectrometry: Instrumentation, applications, and combination with other visualization techniques," *Mass Spectrom Rev*, vol. 35, no. 1, pp. 147–169, 2016, doi: 10.1002/mas.21468.
- [151] A. Macklin, S. Khan, and T. Kislinger, "Recent advances in mass spectrometry based clinical proteomics: applications to cancer research," *Clinical Proteomics*, vol. 17, no. 1, p. 17, May 2020, doi: 10.1186/s12014-020-09283-w.
- [152] L. E. M. Tideman *et al.*, "Automated biomarker candidate discovery in imaging mass spectrometry data through spatially localized Shapley additive explanations," *Analytica Chimica Acta*, vol. 1177, p. 338522, Sep. 2021, doi: 10.1016/j.aca.2021.338522.
- [153] H. Liu *et al.*, "1,5-Diaminonaphthalene Hydrochloride Assisted Laser Desorption/Ionization Mass Spectrometry Imaging of Small Molecules in Tissues Following Focal Cerebral Ischemia," *Anal. Chem.*, vol. 86, no. 20, pp. 10114–10121, Oct. 2014, doi: 10.1021/ac5034566.
- [154] S. A. Schwartz, M. L. Reyzer, and R. M. Caprioli, "Direct tissue analysis using matrix-assisted laser desorption/ionization mass spectrometry: practical aspects of sample preparation," *Journal of Mass Spectrometry*, vol. 38, no. 7, pp. 699–708, 2003, doi: 10.1002/jms.505.